CALPHAD: Computer Coupling of Phase Diagrams and Thermochemistry 82 (2023) 102589

Contents lists available at ScienceDirect

Calphad

journal homepage: www.elsevier.com/locate/calphad

Thermodynamic evaluation and optimization of the As–Co, As–Fe and As–Fe–S systems

Oumaima Kidari *, Patrice Chartrand

Center for Research in Computational Thermochemistry (CRCT) - Polytechnique Montréal, Department of Chemical Engineering, Box 6079, Station Downtown, Montréal, Québec, H3C 3A7, Canada

ARTICLE INFO

Handling Editor: Prof. Z.K. Liu

Keywords:
Thermodynamic modeling
Modified quasichemical model
CALPHAD
Arsenic
Speiss

ABSTRACT

A critical evaluation of all available phase diagram and thermodynamic data for the As–Co and As–Fe binary systems as well as the As–Fe–S ternary system has been performed and thermodynamic assessments over the whole composition ranges are presented using the CALPHAD method. To predict thermodynamic properties and phase equilibria for these systems, the Modified Quasichemical Model (MQM) for short range ordering was used for the liquid phases. The Compound Energy Formalism (CEF) was used for the solid solutions. Since Co and Fe are ferromagnetic, magnetic contributions were added to describe the Gibbs energy of cobalt and iron rich solid solutions. Important uncertainties remain for the liquidus of As-rich regions in the binary subsystems.

1. Introduction

Cobalt and iron are commonly found together in arsenic containing sulfide minerals. Cobalt is a transition metal with many desirable characteristics; it is a ferromagnetic element with unique valency and corrosion resistance over a wide temperature range. Its many properties make it valuable for various applications such as superalloys and ceramics manufacturing as well as lithium-ion batteries. It is also frequently used as a desulphurization catalyst of petroleum [1–5]. Cobalt is strongly siderophile and therefore often associated with iron minerals. Iron is a widely used transition metal due to its ferromagnetic ability, low cost and conductivity [6]. Both cobalt and iron are chalcophile, and since arsenic is very common in sulphide mineralization, the processing of ores containing cobalt and iron minerals can cause major challenges [7]. In fact, arsenic is a very toxic element and sulfide ore processing can be a major source of arsenic contamination to the environment. Arsenopyrite (FeAsS) is a ubiquitous arsenic bearing sulfide mineral, primarily associated with sulfide minerals of mostly copper, silver, and gold [8,9]. Cobalt is found mainly in cobaltite (CoAsS) and it is usually produced as a by-product of processing various metals. The close ionic radius of cobalt and iron and other similarities in their physical properties make iron substitution by cobalt very common. So minerals like glaucodot ((Co, Fe) AsS) and skutterudite ((Co, Ni, Fe)As_3) are widely found in various ores [1,2,10]. To find solutions to reduce toxic arsenic emissions caused by the treatment of complex concentrates, the development of thermodynamic models of compounds and mixtures and their associated databases for arsenic, cobalt, iron, and sulfur systems is advantageous for the sulfide smelting industry. In the present article, the available experimental data of the two binary systems As–Co and As–Fe and the ternary system As–Fe–S is presented and critically evaluated. A set of model parameters is optimized for each phase to predict thermodynamic properties and phase equilibria for these systems using the CALPHAD approach. The Modified Quasichemical Model in the Pair Approximation developed by Pelton et al. [11,12] was used for the liquid phases, and the Compound Energy Formalism (CEF) introduced by Sundman and Ågren [13] was used for solid solutions. All calculations and optimizations in this work were performed with the FactSage™ thermochemical software [14–16]. The previous assessments of As–Fe system by Pei et al. [17] and Ohno and Yoh [18] are presented and discussed briefly. For the As–Fe–S ternary system, the work of Xing et al. [19] presenting thermodynamic models for some ternary solid solutions is also mentioned. The parameters suggested by the previous assessments of Fe–S system by Waldner and Pelton [20] and As–S system by Kidari and Chartrand [21] are added to the present work to evaluate the ternary As–Fe–S systems.

* Corresponding author.
E-mail address: oumaima.kidari@polymtl.ca (O. Kidari).

https://doi.org/10.1016/j.calphad.2023.102589
Received 21 March 2023; Received in revised form 10 July 2023; Accepted 11 July 2023
Available online 21 July 2023
0364-5916/© 2023 The Authors. Published by Elsevier Ltd. This is an open access article under the CC BY license (http://creativecommons.org/licenses/by/4.0/).

Table 1
As–Co phase diagram data reported in the literature.

References	Experimental methods and results
[22]	**TA:** Determination of the phase diagram up to a composition of 48 at. % As.
[23]	**TA, thermal expansion test and magnetic content analysis:** Determination of the phase diagram up to a composition of 28.5 at. % As and determination of the magnetic transition.
[24]	**TA:** Determination of the phase diagram up to a composition of 25 at. % As.
[25]	**Ignition analysis:** Study of the oxidation kinetics and determination of the limits of solid solutions for Co_5As_2, Co_2As, Co_3As_2 and CoAs.
[26]	**Quenching method combined with EPMA:** Determination of the limits of the biphasic liquid + fcc cobalt region between 1273 K and 1473 K.

2. Literature review

2.1. As–Co binary phase diagram

The As–Co system has six intermediate compounds stable at ambient pressure: Co_5As_2, Co_2As, Co_3As_2, CoAs, $CoAs_2$ and $CoAs_3$. The crystal structures of the phases are presented in Table 4. The arsenic rich side of the As–Co phase diagram has not been investigated. The experimental studies measuring phase diagram data for the cobalt rich side are presented in Table 1. Details of these studies are discussed and reviewed in this section.

2.1.1. $Co - Co_5As_2$ subsystem

Solid solubility: The solubility of arsenic in cobalt is not negligible. A maximum solubility of 3 at. % As in Co at 1180 K was measured by Friedrich [22]. For the same temperature, Koster and Mulfinger [24] measured a higher maximum solubility of 5.6 at. % As in Co and estimated that the solubility decreases to at least to 4 at. % As with decreasing temperature. The measured value by Koster and Mulfinger [24] is in agreement with the measurements of the solidus curve by Hino and Azakami [26]. Eutectic: According to Friedrich [22], a eutectic reaction takes place at a temperature of 1189 K to form solid cobalt and Co_5As_2 at a composition around 26 at. % As. This is close to the eutectic temperature of 1193 K measured by Koster and Mulfinger (Koster & Mulfinger, 1938) for the same eutectic composition. Haschimoto [23] measured a higher eutectic temperature of 1270 K. Liquidus: The liquidus curve has been measured up to 25 at. % As by Friedrich [22], Koster and Mulfinger [24], Haschimoto [23] as well as Hino and Azakami [26]. The curve measured by Friedrich [22] is higher than that measured by Koster and Mulfinger [24] and slightly lower than the measurements made by Haschimoto [23] and Hino and Azakami [26]. Magnetism: The Curie temperature of pure fcc Co is lowered from 1396 K to a fixed value of 1198 K in the two-phase region according to Koster and Mulfinger [24] and at a temperature of 1336 K according to Haschimoto [23].

2.1.2. Co_5As_2-CoAs subsystem

The only measurements for this subsystem are made by Friedrich [22]. Also, thermal effects between 13 at. % to 37 at. % As were recorded, for temperatures between 521 K and 625 K. Since a considerable increase in volume occurred at the composition of Co_2As, Friedrich [22] suggested that the thermal effects were probably due to a polymorphic transformation of the compound. According to Hansen and Anderko [27], this assumption is doubtful.

2.1.3. Non-stoichiometry of the intermediate phases

The compounds Co_5As_2, Co_2As, Co_3As_2 and CoAs are not stoichiometric according to Kochner [25]. Based on his measurements of ignition temperatures, a curve was determined, and its evolution shows that when the solubility limit for a compound is reached, the curve evolves horizontally at a constant temperature and rises from the composition of the adjacent arsenide, showing a narrow homogeneity range. Kochner [25] therefore concluded the limits of the following solid solutions: from 27.5 at. % to 30.1 at. % As for Co_5As_2, from 32.7 at. % to 35.8 at. % As for Co_2As, from 39 at. % to 43% molar arsenic for Co_3As_2 and up to 47.6 at. % As for CoAs.

2.1.4. Co_5As_2

Much uncertainty still surrounds the temperature range of the stability of Co_5As_2 and if it exists in more than one structural form. At a temperature of 1101 K, the compound undergoes a polymorphic transformation according to Friedrich [22], but he observed no structural change. The compound is not congruent, and it decomposes by a peritectic reaction at 1196 K. According to Haschimoto [23], the polymorphic transformation of the compound occurs at a temperature of 1139 K, which is higher than the temperature measured by Friedrich [22]. According to the XRD experiments performed by Heyding and Calvert [28], if the compound Co_5As_2 exists, it is only stable at high temperatures, and it decomposes into Co_2As and the fcc Co solid solution above 1073 K. The DTA measurements by Ellner et al. [29] confirmed the existence of Co_5As_2 at high temperatures only, in a range of about 50°. It decomposes at a temperature of 1140 K, 70° lower than the decomposition temperature of Ni_5As_2. According to measurements of Espeleta [30] performed by drop calorimetry between 800 K and 1500 K, there is a polymorphic transformation of Co_5As_2 at a temperature of 1176 ± 3 K. The measured heat of transformation is 27.3 ± 2.5 kJ/mol. Espeleta [30] measured a peritectic temperature of 1224 ± 3 K, and the calculated heat of fusion is 36.7 ± 0.9 kJ/mol. The existence of the compound Co_5As_2 is doubtful according to Elliott [31].

2.1.5. Co_2As

Nylund et al. [32] reported a rhombohedral structure for Co_2As. Heyding and Calvert [28] showed the existence of Co_2As at room temperature in a pseudo-hexagonal form, and after a slow polymorphic transition, a hexagonal form appears between 763 K and 793 K upon heating, and between 661 K and 675 K upon cooling. The XRD results of Kjekshus and Skaug [33] showed a transformation at 725 ± 5 K, which does not agree with the ranges suggested by Heyding and Calvert [28]. They also showed that Co_2As is paramagnetic at temperatures above 60 K. According to Friedrich [22], Co_2As decomposes following a peritectic reaction at 1230 K.

2.1.6. Co_3As_2

At a temperature of 1182 K, Co_3As_2 undergoes a polymorphic transformation according to Friedrich [22]. Also, the compound is not congruent and decomposes by a peritectic reaction at a temperature of 1287 K. This does not agree with the results of Heyding and Calvert [28], which show that Co_3As_2 is stable only at high temperatures, above 1213 K.

2.1.7. CoAs

According to Friedrich [22], CoAs is congruent with a melting temperature around 1453 K. Heyding and Calvert [28] show that the compound exists at room temperature and undergoes a polymorphic transformation, between 1217 K and 1233 K. The transformation takes place at a higher temperature, of 1248 ± 20 K according to the XRD results obtained by Selte and Kjekshus [34], from an orthorhombic structure to a hexagonal structure.

2.1.8. $CoAs_2$

$CoAs_2$ is found as the minerals smaltine and safflorite with a monoclinic structure [35–37]. High temperature investigations by XRD, DTA and quenching experiments performed by Kjekshus and Rakke [38] showed a polymorphic transformation at a temperature of 870 K. According to the thermal-scanning experiments of Siegrist and Hulliger [39], the transformation occurs at 800 ± 2 K upon heating and 797 ± 2 K upon cooling. The corresponding transformation enthalpy is 800

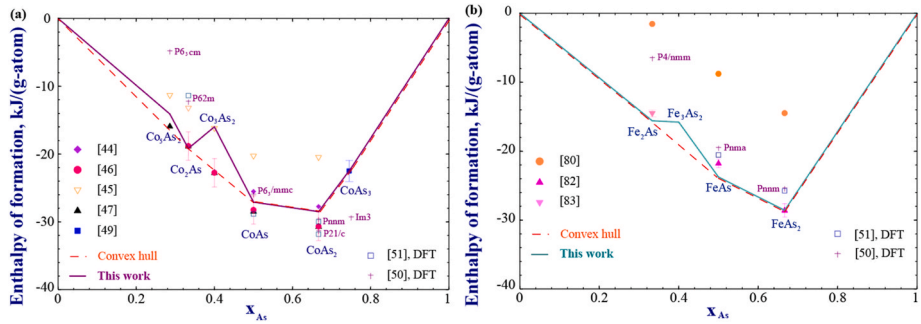

Fig. 1. Enthalpies of formation of intermediate compounds in **a)** As–Co system and **b)** As–Fe system.

J/mol. The melting point of this compound is still uncertain.

2.1.9. $CoAs_3$

$CoAs_3$ corresponds to the mineral skutterudite and it appears to exist in only one cubic form [40]. The melting point of this compound is still uncertain.

2.2. Thermodynamic properties of As–Co binary system

2.2.1. As − Co liquid

Vaisburd and Remen [41] determined the activity of Co in As–Co melt by measuring the emf on concentration cells without transport. The measurements were performed at 1573 K over a composition range of 35–50 at. % As. Hino and Azakami [26] also determined the activity of As in As–Co alloys using the isopiestic method. The measurements were performed at 1273 K and 1423 K over a composition range of 25–50 at. % As, with a conversion to liquid arsenic as the standard state. The measured activities show negative deviation from Raoult's law. The activity data is presented in Fig. 4.

2.2.2. As − Co compounds

There is a lack of direct thermodynamic data measurements for compounds of the As–Co system. Niessen et al. [42] and Hisham and Benson [43] estimated the standard heats of formation of some of the compounds in this binary system but the estimated values seem unreliable given the disagreement between their estimates and measured enthalpy values of other known compounds. Standard heats of formation of some compounds were also listed in the thermodynamic tables by Naumov et al. [44], Wagman et al. [45], Kubaschewski et al. [46] and Smithells and Brandes [47]. The methods used to obtain these values have not been listed, apart from Kubaschewski et al. [46] who cited the work of Kochnev [48]. Kochnev [48] studied the thermal dissociation of Co_5As_2, Co_2As, Co_3As_2, CoAs, Co_2As_3 and $CoAs_2$ by determining the pressure of As_4 by the molecular flow method at a certain temperature for each compound. It was assumed that arsenic vapors under these conditions obey the laws of ideal gases, and all thermodynamic equations derived for ideal gases were used to calculate the heats of formation. Kochnev [48] explains that his work is only approximative since the dissociation products were partially dissolved in the primary arsenide during the experiments and the total weight loss during several experiments was around 0.6%. The heat content of Co_5As_2 was determined using drop calorimetry by Espeleta et al. [30] over a temperature range of 800 K–1500 K. Temperature coefficients of the heat content were then determined with a regression analysis method using the Shomate function, from which the heat capacity at high temperatures was derived. The standard enthalpy of formation value suggested for Co_5As_2 is -435.7 ± 54.1 kJ/mol. This value is much more negative than the value of -270.9 kJ/mol estimated by Klingbeil et al. [27] using the Miedema model which tends to overestimate the standard heats of formation. For $CoAs_{2.92}$, Majzlan [49] recently determined a standard enthalpy of formation value of -88.2 ± 6.1 kJ/mol using high-temperature oxide-melt solution calorimetry. Fig. 1 presents the standard enthalpies of formation reported in the literature for the compounds in the As–Co system including the DFT values reported in The Materials Project [50] and the Open Quantum Materials Database [51]. Majzlan [49] also measured the heat capacity of $CoAs_{2.92}$ using relaxation calorimetry (PPMS) between 2 K and 303 K and using DSC between 280 K and 366 K. The measurements had to be stopped upon reaching 366 K because the data became unusually scattered. The DSC values were slightly higher than the PPMS values in the overlap region. The calculated heat capacity curves for the compounds in the As–Co system are presented in Fig. 2 and the standard entropies at 298.15 K are presented in Fig. 3.

2.3. As–Fe binary phase diagram

The As–Fe system has three stoichiometric intermediate compounds stable at ambient pressure: Fe_2As, FeAs and $FeAs_2$. The crystal structures of the phases are presented in Table 4. The Experiments of Friedrich and Borchers [52] and Sawamura et al. [53] also indicated the existence of a high temperature solid solution around a composition of Fe_3As_4. Just like for the As–Co system, measurements in the arsenic-rich side of the

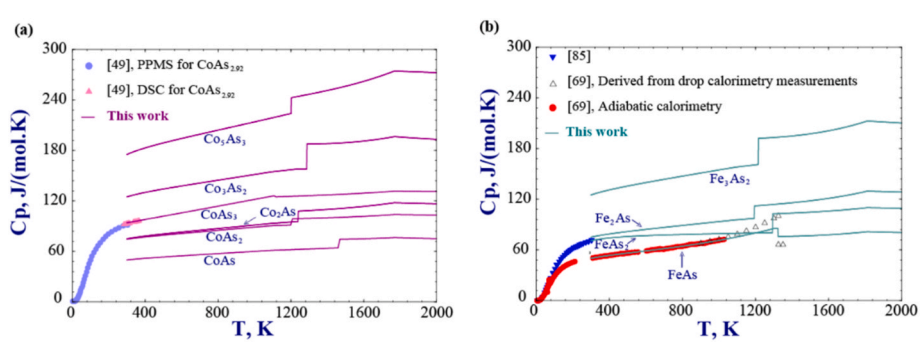

Fig. 2. Calculated heat capacity of compounds of the **a)** As–Co system, **b)** As–Fe system.

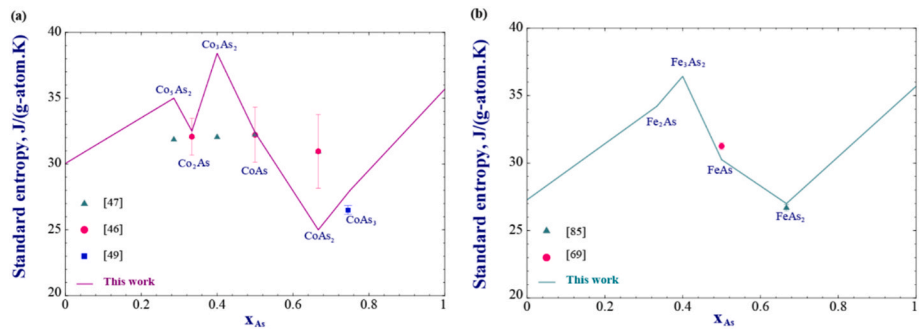

Fig. 3. Standard entropies of the intermediate compounds in **a)** As–Co, **b)** As–Fe systems.

Table 2
As–Fe phase diagram data reported in the literature.

References	Experimental methods and results
[52]	**TA and metallography:** Determination of the phase diagram between the compositions of 6 at. % and 49 at. % As.
[54]	**TA, metallography, and magnetic content analysis:** Determination of the phase diagram up to a composition of 32 at. % As and determination of the magnetic transition.
[55]	**Diffusion measurement of arsenic in iron:** Determination of the saturation composition of iron (fcc) at 1423 K.
[56]	**Dilatometric, metallography and XRD:** Determination of the limits of the iron (fcc) saturation loop.
[57]	**TA and metallography:** Suggestion of the solubility of arsenic in iron (fcc) based on extrapolations from measurements made on alloys of iron and arsenic containing low concentrations of carbon.
[53]	**DTA:** Determination of the phase diagram between the compositions of 40 at. % and 57 at. % As.
[58]	**Magnetic content analysis: D**etermination of the magnetic transition.
[59]	**TA, metallography and XRD:** Determination of the limits of the iron (fcc) saturation loop.
[60]	**Microhardness, metallography and XRD:** Determination of the solid solubility of arsenic in iron (bcc).
[61]	**TA:** Determination of phase diagram data for two alloys at compositions of 58 at. % and 70 at. % As.
[62]	**DTA:** Determination of the solid solubility of arsenic in iron (bcc).
[63]	**TA:** Determination of the maximum solid solubility of arsenic in iron (bcc) at the eutectic temperature.

As–Fe system were difficult to obtain. The experimental studies measuring phase diagram data are presented in Table 2. Details of these studies are discussed and reviewed in this section.

2.3.1. *Fe − Fe_2As subsystem*

Fe loop: The fcc form of iron becomes unstable and the bcc form becomes stable after arsenic additions. The solubility limit of arsenic in fcc iron is therefore limited by a closed loop according to Wever [64]. At 1423 K, the saturated fcc iron solution contains approximately 2.8 at. % As as measured by Jones [55]. For the same temperature, the extrapolation by Sawamura et al. [57] showed a saturation composition of 1.65 at. % As. The limits of the region Fe (fcc) + Fe (bcc) were measured by Svechnikov and Gridnev [56], between 1.1 and 1.9 at. % As at a temperature of 1273 K and between 1.8 and 2.5 at. % As at 1373 K. Solid solubility: Friedrich and Borchers [52] measured a maximum solid solubility of 6 at. % As in bcc Fe at the eutectic temperature, Oberhoffer and Gallaschik [54] measured a maximum value of 5.1 at. % As and Sawamura et al. [57] measured a maximum value of 8.4 at. % As at the eutectic temperature. These three values were not obtained under equilibrium conditions according to Hansen and Anderko [27]. Svchnikov and Shurin [59], Predel and Fredel [62] and Bovzic and Lucic [65] measured a higher solid solubility around 10 at. % As at the eutectic temperature. Eutectic: Oberhoffer and Gallaschik [54] concluded that a peritectic reaction Liquid + Fe (bcc) ⇄ Fe (fcc) takes place at a temperature of 1713 K. This conclusion is not supported by convincing evidence according to Hansen and Anderko [27]. According to the experiments of Friedrich and Borchers [52], a eutectic reaction takes place between 1106 K and 1041 K to form Fe_2As and the bcc Fe solid solution at a composition around 24.4 at. % As. This agrees with the eutectic temperature of 1100 K and the eutectic composition of 25.2 at. % As measured by Oberhoffer and Gallaschik [54]. A slightly higher eutectic temperature of 1113 K was measured by Sawamura et al. [57] with a eutectic composition of 24 at. % As. The eutectic temperature according to Bozic and Lucic is 1118 ± 5 K. Liquidus: Friedrich and Borchers [52] and Oberhoffer and Gallaschik [54] both measured the liquidus and they are in good agreement. Magnetism: Oberhoffer and Gallaschik [54] performed measurements to determine the magnetic transformation of iron containing less than 1.7 at. % As. According to their results, the magnetic transition in the Fe (bcc)-Fe_2As region is constant at 1041 K upon heating. However, the temperature of the magnetic transformation decreases upon cooling and the difference is about 60°. The magnetic transformation temperature during heating by Oberhoffer and Gallaschik [54] agrees with the results obtained by Sawamura et al. [58] who measured the same temperature during heating and cooling; constant at 1041 K up to a composition of 3 at. % As. The temperature then gradually decreases until it reaches 1003 K C at 7.65 at. % As.

2.3.2. *Fe_2As-FeAs subsystem*

Friedrich and Borchers [52] and Sawamura et al. [58] also measured phase diagram data from Fe_2As to FeAs compositions. Based on their measurements, Friedrich and Borchers [52] suggested the formation of a high temperature solid solution with a composition around Fe_3As_2. The solid solution decomposes at a temperature of 1073 K. However, the XRD and the microscopic investigation by Hagg [66] failed to find the Fe_3As_2 solid solution while Hagg [67] confirms that it does not exist at temperatures lower than 1068 K. According to the experiments of Sawamura et al. [58], a solid solution identified as ε exists, but it could not be confirmed whether it corresponds to Fe_3As_2. The ε phase forms by a peritectic reaction (Liquid + FeAs ⇌ ε) at a temperature of 1275 K at 42.1 at. % As. The phase decomposes by a eutectoid reaction (ε ⇌ Fe_2As + FeAs) at a temperature of 1097 K at. 40 at. % As. Alloys quenched from temperatures above 1073 K by Heyding and & Calvert [28] did not indicate the presence of the Fe_3As_2 phase. Also, according to the PXRD experiments by Seitkan et al. [68], there is no evidence of the presence of the Fe_3As_2 phase at temperatures between 1068 K and 1122 K.

2.3.3. *FeAs-$FeAs_2$ subsystem*

Clark [61] performed a single measurement for this subsystem at a composition of 58 at. % As, corresponding to the eutectic temperature of 1281 ± 5 K.

2.3.4. *$FeAs_2$-As subsystem*

According to Clark [61], the eutectic composition is greater than 93.5 at. % As and the eutectic temperature around 1073 ± 10 K. The solubility of Fe in As was estimated at 99.93 at. % As at the eutectic temperature.

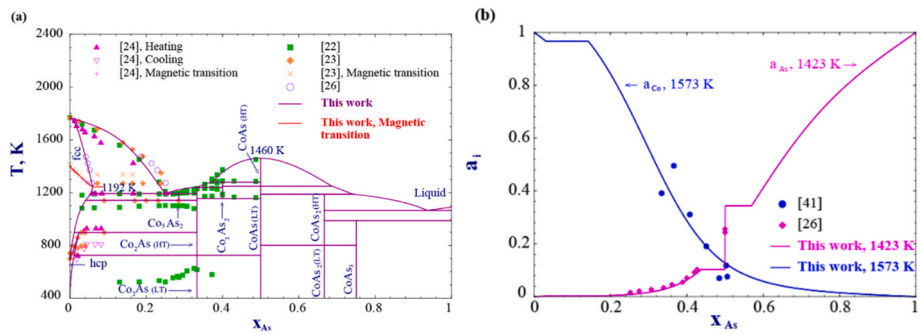

Fig. 4. Calculated **a)** As–Co phase diagram, **b)** activities of As and Co in As–Co system, with solid cobalt and liquid arsenic standard states.

2.3.5. Fe_2As

No natural occurrence is known for Fe_2As. This compound has a tetragonal structure [67]. Its melting point is 1192 K according to Friedrich and Borchers [52]. A higher temperature of 1203 K was measured by Sawamura et al. [53].

2.3.6. FeAs

No natural occurrence is known for FeAs. This compound has an orthorhombic structure [66]. Its melting point is 1281 ± 5 K according to Clark [61]. A higher temperature of 1325 K was measured by Gonzalez-Alvarez et al. [69] who also observed a transition where the magnetic helical structure disappears at a temperature of 70.95 ± 0.02 K.

2.3.7. $FeAs_2$

$FeAs_2$ corresponds to the mineral loellingite with an orthorhombic structure [70]. Heyding and Calvert [71] observed the phase with a minor arsenic defficiency but without quantifying it. The melting point of this phase is 1289 ± 8 K.

2.4. Thermodynamic properties of As–Fe binary system

2.4.1. As – Fe liquid

The activity of Fe in As–Fe melt was determined by Vaisburd and Remen [41] by measuring the emf on concentration cells without transport. The measurements were performed at 1573 K over a composition range of 11–47 at. % As. Hino and Azakami [72] determined the activity of As in As–Fe alloys using the isopiestic method. The measurements were performed at 1423 K over a composition range of 20–50 at. % As, with a conversion to liquid arsenic as the standard state. Arsenic properties used in their calculation are from Hultgren et al. [73]. Botor et al. [74] also determined the activity of As in As–Fe alloys based on vapor pressure measurements using two effusion methods: the Knudsen method and the Knudsen cell-mass spectrometry method. The measurements were performed over the temperature range of 1198 K and 1580 K from 21 to 35 at. % As and over the range of 1624 K and 2013 K from 0.99 to 10 at. % As. Arsenic properties used in their calculation are from Gokcen et al. [75]. Botor et al. [74] also recalculated the arsenic activity from the results of Hino and Azakami [72] using arsenic properties from Gokcen et al. [75]. The recalculated values as well as the original values by Hino and Azakami [72] are higher than those determined based on the vapor pressure measurements of Botor et al. [74]. Dong et al. [76] calculated activity coefficients of As and Fe at 1873 K using the method of free energy of fusion for alloys with compositions up to 24 at. % As. Tsukihashi et al. [77] also determined activity coefficients of As in pure Fe between 1823 K and 1923 K relative to pure liquid using chemical equilibration technioque. Yan et al. [78] calculated the activity of As and Fe in the As–Fe system using a combination of the molecular interaction volume model, Miedema's semi-empirical enthalpy model and the Tanaka equation. Their calculations are in good agreement with the activity values from Hino and Azakami [72] and Dong et al. [76]. Like the activities in the As–Co system, all measured activities in the As–Fe system show strong negative deviation from Raoult's law. The activity data is presented in Fig. 5. At at a temperature of 1123 K, Wypartowicz et al. [79] performed three experiments measuring the liquid enthalpy of mixing at the eutectic composition of 24 at. % As using high temperature drop calorimetry. The obtained values were −11.7, −12.1 and −14.1 kJ/mol.

2.4.2. As – Fe compounds

No thermodynamic data available for Fe_3As_2. For Fe_2As, FeAs and $FeAs_2$, Barton [80] suggested standard heat of formation values based on extrapolations of phase equilibrium measurements for the ternary system As–Fe–S from 773 K to 1073 K. According to Perfetti et al. [81], the extrapolations of Barton [80] present significant uncertainties. Stolyarova [82,83] measured the heat of formation of Fe_2As, FeAs and $FeAs_2$ using high-temperature calorimetry and as seen from Fig. 1, the values are higher than those suggested by Barton [80]. The heat content of $FeAs_2$ was determined using drop calorimetry by Espeleta et al. [30] over a temperature range of 800 K–1500 K. From the measurements Espeleta et al. [30] calculated a standard heat of formation value of 114.3 ± 17.2 kJ/mol. This value is much higher than the value 86 ± 3

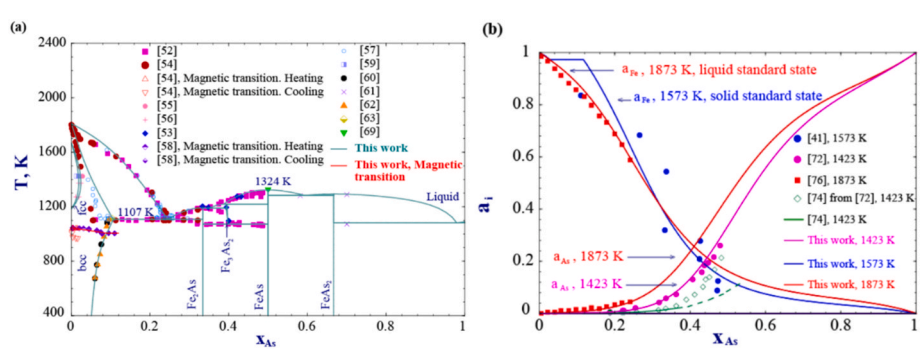

Fig. 5. Calculated **a)** As–Fe phase diagram, b) activities of As and Fe in As–Fe system, with solid iron, liquid iron and liquid arsenic standard states.

Table 3
As–Fe–S phase diagram data reported in the literature.

References	Experimental methods and results
Fe_2As-FeS	
[92]	**TA, XRD and microscopic examination:** Determination of the quasi-binary section for the entire composition range.
Isothermal sections	
[61,93]	**Evacuated, sealed silica tubes experiments, XRD and optical examination:** Determination of equilibrium phase relations at 873 K, and changes in assemblages between 673 K and 1023 K.
[80]	**Quenching experiments, XRD, optical examination and pyrrhotite-indicator method:** Determination of four-phase invariant reactions during solidifications and prediction of isothermal sections between 554 K and 1103 K.
[94]	**Based on literature descriptions of natural assemblages:** Proposition of a As–Fe–S phase diagram.
[95]	**Sub-solidus recrystallization experiments, microprobe analysis and XRD:** Determination of the composition and phase relations involving FeAsS.
Liquidus surface	
[91]	**Based on the work of Clark [61] and Barton [80]:** Suggestion of a schematic liquidus surface.

kJ/mol by Stolyarova [82]. Niessen et al. [42] and Klingbeil et al. [84] estimated the standard heats of formation of some compounds in the As–Fe binary system using Miedema's model but their values are overestimated compared to the measured values. Fig. 1 also shows the enthalpy of formation of some compounds at 0 K obtained from DFT calculations reported in The Materials Project [50] and The Open Quantum Material Database (OQMD) [51]. Espeleta et al. [30] determined the temperature coefficients of the heat content by a regression analysis method using the Shomate function, from which the heat capacity of Fe_2As at high temperatures was derived. No heat capacity measurements were found for this compound. Gonzalez-Alvarez et al. [69] measured the heat capacity of FeAs using adiabatic calorimetry over the range 5 K–1030 K and using drop calorimetry relative to 298.15 K over the range 875 K–1350 K. Pashinkin et al. [85] measured the heat capacity of $FeAs_2$ for temperatures between 5 K and 300 K using adiabatic calorimetry. For higher temperatures. Perfetti et al. [81] estimated the heat capacity of $FeAs_2$ by analogy with the heat capacity of isostructural FeS_2 (marcasite) and FeAsS (arsenopyrite). The heat capacity data for the compounds in the As–Fe system are presented in Fig. 2 and the standard entropies are presented in Fig. 3.

2.5. Thermodynamic assessments of As–S, As–Co, As–Fe and Fe–S binary systems in the literature

No previous assessment was found for the binary As–Co system. Using the PARROT program [86], the binary As–Fe system was previously assessed by Pei et al. [17] with an ionic two-sublattice model for the liquid phase and a substitutional regular solution model for the terminal bcc Fe and fcc Fe solid solutions. Ohno and Yoh [18] developed a thermodynamic model combined with first-principles total energy calculations based on the projector augmented wave (PAW) method [87] within the generalized gradient approximation (GGA) [88]. The liquid phase was described using a substitutional solution model. The assessment of thermodynamic properties of the As–Fe system was also performed by Botor et al. [74] using the NRTL model and by Yan et al. [78] using a combination of the molecular interaction volume model, the Miedema's semi-empirical enthalpy model et the Tanaka equation [89]. Thermodynamic modeling of the As–S binary system was performed by Prostakova et al. [90] using the Modified Quasichemical Model (MQM) for the liquid phase. A subsequent and improved thermodynamic model of the As–S binary system was performed by Kidari and Chartrand [21] including three intermediate stoichiometric compounds stable at atmospheric pressure: As_2S_3, As_4S_4 et As_4S_3. Thermodynamic modeling of the Fe–S binary system was performed by Waldner and Pelton [20], and according to their model, the system includes six intermediate stoichiometric compounds stable at atmospheric pressure: FeS (troilite), $Fe_{11}S_{12}$, $Fe_{10}S_{11}$, Fe_9S_{10}, Fe_7S_8 (monoclinic pyrrhotite) and FeS_2 (pyrite). The system also includes the $Fe_{1-x}S$ (pyrrhotite) solid solution that exhibits a substantial deviation from stoichiometry toward excess S. For both As–S and Fe–S binary systems, the calculations and optimizations were performed with the FactSage™ thermochemical software [14–16]. The Modified Quasichemical Model (MQM) was used for the liquid phase and the compound energy formalism (CEF) was used to model the pyrrhotite solution. The optimized parameters of the As–S system in our previous work [21] and the Fe–S system by Waldner and Pelton [20] are used in this work to evaluate the ternary As–Fe–S system.

2.6. As–Fe–S ternary phase diagram

Several investigations examined the As–Fe–S system, contrary to the less studied As–Co–S system. FeAsS is the only known compound in the As–Fe–S ternary system [91], and the studies concerning this ternary system are presented in Table 3 and discussed in this section.

2.6.1. Fe_2As-FeS pseudo-binary system

According to the measurements performed by Nishihara and Izaki [92], a eutectic reaction forming $Fe_2As + FeS$ occurs at a temperature of 1154 K and a composition around 22.5 mol % FeS. Also, a monotectic reaction occurs at a temperature of 1323 K. The mutual solid solubility of Fe_2As and FeS could not be measured.

2.6.2. As–Fe–S isothermal sections

Based on mineral occurrences reported in the literature, McKinstry [94] proposed a As–Fe–S ternary phase diagram without considering the phases FeAs and Fe_2As. According to Clark [93], tie-lines change as function of deposition temperature and pressure, and since the proposed phase diagrams by McKinstry [94] is based on a series of isolated mineral occurrences, it may include assemblages that are not stable at any given temperature. Clark [61,93] investigated phase relations in the synthetic As–Fe–S ternary system and the measurements were performed with the presence of vapor. Vapor pressures could not be measured, and Clark [61] assumed that the pressures of all vapors in equilibrium with condensed phases lie between 1.3×10^{-14} and 6.5 bar at 873 K. The determined isothermal diagram at 873 K shows eight univariant four-phase assemblages. Clark [61] also studied the changes in stable phases and produced five isothermal sections in the following temperature ranges: $T < 764 \pm 12$ K, 764 ± 12 K $< T < 961 \pm 3$ K, 961 ± 3 K $< T < 975 \pm 3$ K, 975 ± 3 K $< T < 1016 \pm 2$ K and $T > 1016 \pm 2$ K. Barton [80] measured five ternary univariant equilibria in presence of vapor and the proposed isothermal ternary diagrams are in good agreement with the work of Clark [61]. Based on the results of Clark [93] and Barton [80], Raghavan [91] suggested a liquidus surface. In addition to the liquid miscibility gap on the FeS-Fe_2As pseudo-binary system, Raghavan [91] suggests another liquid miscibility gap originating along the Fe–S side and extending to the As corner.

2.6.3. Fe solubility in As–S liquid

Since orpiment (As_2S_3) and realgar (As_4S_4) melt at temperatures slightly above 573 K, Clark [93] reported a very narrow liquid field extending along the As–S binary system. The solubility of iron could not be measured, but according to previous measurements by Drs. Wiik and Paavo Vaananen (cited in Ref. [61]), liquid As–S contains around 0.16 at. % Fe.

2.6.4. FeAsS

FeAsS correspond to the naturally occurring mineral arsenopyrite. Like the structure of loellingite ($FeAs_2$), the structure of arsenopyrite also derives from the structure of marcasite (FeS_2), a polymorph of

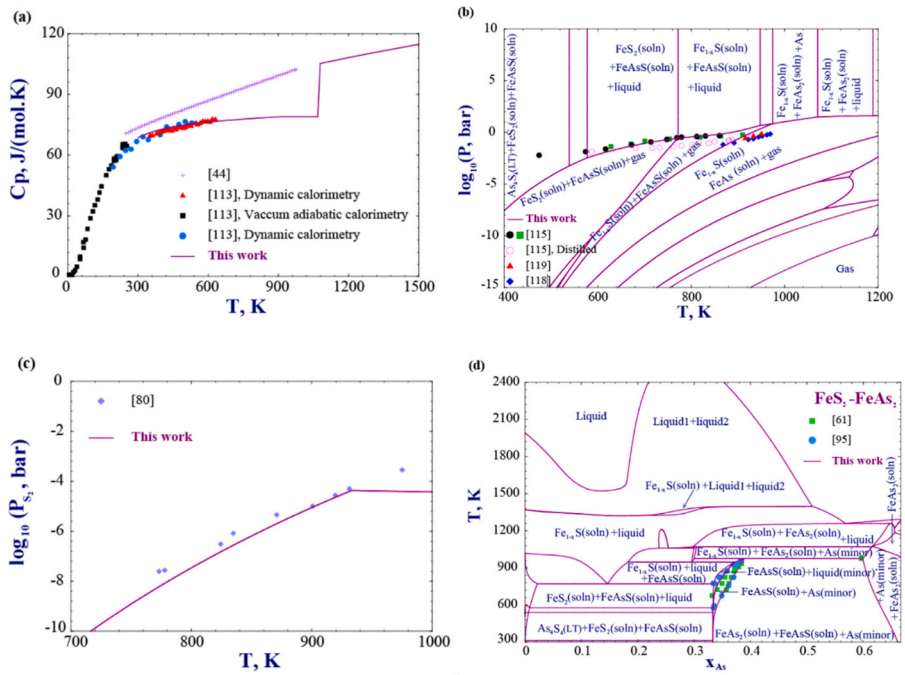

Fig. 6. Calculated **a)** heat capacity of AsFeS, **b)** vapor pressures of AsFeS, **c)** activity of S_2, **d)** FeS_2-$FeAs_2$ join.

pyrite [96]. Arsenopyrite with the ideal stoichiometry is monoclinic [70], and the deviation from the ideal chemical formula results in a triclinic structure [70,97]. Twining in arsenopyrite gives rise to a pseudo-orthorhombic structure [70,98]. Analyses by Klemm [99] and Kretschmar and Scott [95] showed that naturally occurring arsenopyrite may be slightly iron deficient, less than 1 at. %. However, according to Marimoto and Clark [98], the variations of iron content in arsenopyrite represent sampling and analytical errors rather than a deficiency. Clark [61] investigated the composition of synthetic arsenopyrite and found that it exists over a range of As and S. At 873 K, synthetic arsenopyrite has a small solid solubility and it does not encompass the ideal stoichiometric composition FeAsS. The approximate limits suggested are $FeAs_{1.08}S_{0.92}$ and $FeAs_{1.05}S_{0.95}$. Chemical analysis on natural arsenopyrite performed by Clark [61] showed that it is sulfur rich relative to the ideal stoichiometric formula. The composition is found to be around $FeAs_{0.97}S_{1.06}$. Kretchmar and Scott [95] determined the compositions of arsenopyrite in different assemblages. The measurements are more precise in the assemblage arsenopyrite + pyrrhotite + liquid + vapor and arsenopyrite + pyrrhotite + loellingite + vapeur. For other assemblages, it was more difficult to find arsenopyrite grains suitable for analysis. At 573 K, their results show that the composition range of arsenopyrite extends from less than 30 at. % As in equilibrium with pyrite and arsenic to approximately 33.5 at. % As in equilibrium with pyrrhotite and loellingite. Kretchmar and Scott [95] also showed that arsenopyrite contains around 38.5 at. % As at 973 K. According to Clark [61], arsenopyrite is incongruent and stable up to a temperature of 975 ± 3 K before decomposing to form pyrrhotite, loellingite and liquid. The homogeneity range of AsFeS is shown in Fig. 6 d).

2.6.5. Solubility of As in FeS_2

Thermodynamic modeling of the Fe–S binary system was performed by Waldner and Pelton [20], and their model includes the intermediate stoichiometric compound FeS_2. Natural pyrite (FeS_2) exists in various geological environments, and depending on the hydrothermal conditions, it can incorporate arsenic in a wide composition range [100,101]. Pyrite is reported in deposits with and without the presence of arsenopyrite. In assemblages of pyrite and arsenopyrite, arsenic content was found to vary from sample to sample, ranging from below the detection limit to about 5.2 at. % As in pyrite. Stepanov et al. [101] presents a literature survey detailing the results of the various experimental studies of arsenic content in pyrite in assemblages containing pyrite and arsenopyrite. In deposits without arsenopyrite, arsenic content in pyrite was also found to vary largely, reaching much higher arsenic values around 10.5 at. % As [102]. Few experiments synthesised pyrite and studied its arsenic content. At low temperatures, the nucleation of pyrite does not proceed at a significant rate, making it difficult to obtain an equilibrium state experimentally [103–105]. Low temperature experiments at 573 K–773 K by Fleet and Mumin [106] synthetized metastable pyrite with an arsenic content of up to 5 at. % As. At higher temperatures, lower arsenic contents were reported. According to Clark [61], very little arsenic is soluble in pyrite coexisting with pyrrhotite and the As–S liquid. The value does not exceed 0.28 at. % As at 873 K. Kretchmar and Scott [95] agree with this value. At 773 K, Hem and Makovicky [107] produced nickel and cobalt bearing pyrite in equilibrium with arsenopyrite. Pyrite contained from 0.1 at. % to 4.5 at. % As. Using first principles and monte Carlo calculations, Reich and Becker [108] investigated the thermodynamic mixing properties of As into pyrite. According to their predictions, pyrite can incorporate up to 3 at. % As in solid solution before unmixing into pyrite + arsenopyrite.

2.6.6. Solubility of As in $Fe_{1-x}S$

Thermodynamic modeling of the Fe–S binary system was performed by Waldner and Pelton [20], and their model includes the pyrrhotite $Fe_{1-x}S$ solid solution. Clark [61] examined the solid solubility of arsenic in synthetic pyrrhotite with the composition $Fe_{0.92}S$ and found no evidence of As solubility in pyrrhotite at 873 K. XRD measurements performed by Barton [80] on pyrrhotites from arsenic and arsenic-free charges showed an agreement with the results of Clark [61]. The analyses by Foley and Ayuso [109] also show that arsenic substitutes as a minor element in natural pyrrhotite, no more than 0.06 at. % As according to the chemical analysis of Ettler and Johan [110].

2.6.7. Solubility of S in Fe_2As and FeAs

Sulfur may be slightly soluble in Fe_2As and FeAs according to Clark [61] but the exact amount was not determined.

2.6.8. Solubility of S in $FeAs_2$

The solubility of sulfur in $FeAs_2$ reaches a maximum of 7 at. % S at 975 K and drops slightly at 923 K according to Clark [61]. The solubility can reach up to 0.21 at. % S in natural samples [111].

2.7. Thermodynamic properties of As–Fe–S ternary system

2.7.1. Activity measurements

Using the isopiestic method, the iso-activity of arsenic in Fe–S–As ternary alloys was measured by Hino [112] at a temperature of 1423 K. Arsenic activity has been found to increase with increasing sulfur content. The iso-activity lines of arsenic referred to liquid As as the standard state are shown in Fig. 1.

2.7.2. FeAsS

Naumov et al. [44] proposed an estimation of the heat capacity of arsenopyrite in the temperature range from 248 K to 975 K and subsequently, Pashinkin et al. [113] determined experimentally the heat capacity of arsenopyrite at a composition of $FeAs_{1.08}S_{0.92}$ in the temperature range from 5 K to 620 K. The heat capacity was measured using vacuum adiabatic calorimetry from 5 K to 250 K, using dynamic calorimetry from 55 K to 530 K and using DSC from 350 K to 620 K. The measurements were then stopped because of the noticeable thermal dissociation of arsenopyrite starting from 700 K to 750 K. The data obtained by Pashinkin et al. [113] is in good agreement in the overlapping regions. However, the estimation by Naumov et al. [44] gives higher heat capacities then what was measured by Pashinkin et al. [113]. Based on the phase equilibrium study results, Barton [80] estimated a value of −92.7 kJ/mol for the standard heat of formation of arsenopyrite. Pashinkin et al. [113] calculated a higher value of −108.6 kJ/mol at the stoichiometric composition. Barton [80] also estimated a standard entropy value of 103.8 J/(mol.K). This value is overestimated according to Pashinkin et al. [113], who calculated a value of 68.49 ± 0.9 J/(mol.K) for arsenopyrite at the stoichiometric composition. Pashinkin et al. [113] explains that arsenopyrite is formed by partial substitution of sulfur atoms by arsenic in FeS_2 resulting in a less symmetrical structure. And by comparing the obtained standard entropy to the values of pyrite (53.89 ± 0.47 J/(mol.K)), the order of magnitude corresponds to the replacement of one sulfur atom by a heavier arsenic atom.

For temperatures between 773 K and 975 K, Barton [80] measured the activity of S_2 using the pyrrhotite-indicator method [114] during the following sulfidation reaction involving arsenopyrite:

$$2FeAs_2 + 2FeS + S_2 \rightarrow 4FeAsS \quad (1)$$

The data is presented in Fig. 6. Strathdee and Pidgeon [115] measured the vapor pressure over arsenopyrite using quartz spoon gauge. The thermal decomposition of arsenopyrite occurs according to reaction 2, and in the presence of pyrite, reaction 3 also occurs according to Strathdee and Pidgeon [115]:

$$4FeAsS_{(s)} \rightarrow 4FeS_{(s)} + As_{4(g)} \quad (2)$$

$$4FeAsS_{(s)} + 4FeS_{2(s)} \rightarrow 8FeS_{(s)} + As_4S_{4(g)} \quad (3)$$

Three sets of measurements were performed for temperatures between 473 K and 923 K. The measurements using two different arsenopyrite sample sizes are in good agreement. Another run was also performed using partially distilled arsenopyrite at 873 K to remove some of the volatile sulfur from the sample. The measurements show a "break" which was explained as the point separating the equilibrium between arsenic vapor and liquid As_4S_4 and the equilibrium between arsenic vapor and gaseous As_4S_4. The interpretation of the present phases seems to be erroneous according to Chakraborti and Lynch [116]. Fushimi and Webster [117] also noted that FeS in reaction 2 should be given as $Fe_{1-x}S$. Using the thermographic method, Zviadadze and Rtskhiladze [118] also measured the vapor pressure between 640 K and 677 K. The measurements of Strathdee and Pidgeon [115] and Zviadadze and Rtskhiladze [118] are difficult to interpret according to Barton [80] because the equilibrium is difficult to obtain at temperatures of the order of 773 K. For temperatures between 868 K and 969 K, Pashinkin et al. [119] measured the dissociation pressure of natural arsenopyrite with a composition of $FeAs_{0.96}S_{1.04}$ using a static method with a membrane zero-manometer. The obtained data is in good agreement with the measurements of Zviadadze and Rtskhiladze [118]. The vapor pressure data is presented in Fig. 6.

2.8. Thermodynamic modeling of As–Fe–S ternary system in the literature

Using the SELEKTOR software [120], Vilor et al. [121] performed thermodynamic analysis and numerical simulation of mineral formation in the system Fe–As–S–Cl–Na-H_2O, where the composition of parageneses including arsenopyrite (FeAsS) and pyrite (FeS_2) was calculated. Xing et al. [19] presented thermodynamic models of solid solutions for arsenic in pyrite and arsenic in arsenopyrite contained in gold ores under hydrothermal conditions using the HCh software [122]. But according to Stepanov [123], some predictions of their thermodynamic model are inconsistent with observations in both natural samples and experimental data.

3. Thermodynamic modeling

All calculations and optimizations in this work were performed with the FactSage™ thermochemical software [14–16]. The properties of pure solid and liquid As, Co and Fe are from SGTE [124]. The properties of the gaseous species S, S_2, S_3, S_4, S_5, S_6, S_7 and S_8 are taken from JANAF Thermochemical Tables [125]. The properties of the gaseous species As, As_2, As_3 and As_4 are from Degterov et al. [126] and other of their unpublished optimisations and evaluations. The properties of the gaseous species AsS and As_4S_4 are from Barin [127] based on the calculations of Mah [128]. The properties of gaseous Co and Fe are from Barin et al. [129] and the properties of gaseous FeS are from JANAF Thermochemical Tables [125].

3.1. Thermodynamic model for the liquid phase in the As–Co an As–Fe binary systems

The Modified Quasichemical Model in the Pair Approximation [11, 12] was used to model the liquid phases to take into account the short-range ordering (SRO). For a liquid binary A-B system, the following pair exchange reaction is considered between the A and B atoms on neighbouring lattice sites:

$$(A-A) + (B-B) = 2(A-B)\ ;\ \Delta g_{AB} \quad (4)$$

$(i-j)$ represents the first nearest neighbor (FNN) atom pairs, and Δg_{AB} is the non-configurational Gibbs energy change for the formation of 2 mol of $(A-B)$ pairs. The pair and the overall mole (site) fractions are defined respectively as:

$$X_{ij} = \frac{n_{ij}}{(n_{AA} + n_{BB} + n_{AB})} \quad (5)$$

$$X_A = \frac{n_A}{(n_A + n_B)} = 1 - X_B \quad (6)$$

n_A, n_B represent the number of moles of A and B, n_{AB} represents the number of moles of pairs (A-B). If the coordination number of A is Z_A, the "coordination equivalent" fraction of A is defined as:

$$Y_A = \frac{Z_A n_A}{Z_A n_A + Z_B n_B} = \frac{Z_A X_A}{Z_A X_A + Z_B X_B} = 1 - Y_B = X_{AA} + \frac{X_{AB}}{2} \quad (7)$$

The "coordination equivalent" fraction of B is defined similarly. The Gibbs energy of the binary liquid is given by the following equation:

Table 4
Crystallographic description of the phases in As–Co and As–Fe systems and sublattice models selected for solid solutions in the As–Fe–S system.

Phase	Person symbol	Space group	Prototype	Reference	Sublattice models
Co_5As_2	*hP*42	$P6_3/mmc$		[29]	stoichiometric
Co_2As (HT)	*hP*9	$P\bar{6}2m$		[28]	stoichiometric
Co_2As (LT)	-	–		–	stoichiometric
Co_3As_2	-	–		–	stoichiometric
CoAs (HT)	*hP*4	$P6_3/mmc$		[34]	stoichiometric
CoAs (LT)	*oP*8	$Pna2_1$		[34]	stoichiometric
$CoAs_2$ (HT)	*oP*6	Pnnm		[38]	stoichiometric
$CoAs_2$ (LT)	*mP*12	$P2_1/c$		[36]	stoichiometric
$CoAs_3$	*cI*32	$Im\bar{3}$		[40]	stoichiometric
$FeAs_2$	*oP*6	Pnnm		[70]	$(Fe, Va)_1(As, S)_2$
FeAs	*oP*8	Pnma		[66]	stoichiometric
Fe_3As_2	-	–		–	$(Fe)_3(As, Va)_2$
Fe_2As	*tP*6	$P4/nmm$		[67]	stoichiometric
FeS_2 (pyrite)	*cP*12	Pa3		[151]	$(Fe)_1(S, As)_2$
FeAsS	*mP*12	$P2_1/c$		[39]	$(Fe)_1(As, S)_1(S, As)_1$

$$G = \left(n_A g_A^{\circ} + n_B g_B^{\circ}\right) - T\Delta S^{configuration} + \left(\frac{n_{AB}}{2}\right)\Delta g_{AB} \tag{8}$$

g_A° and g_B° are the molar Gibbs energies of the pure liquid components, and $\Delta S^{configuration}$ is the configurational entropy of mixing given by randomly distributing the (A-A), (B–B) and (A-B) pairs. The non-configurational Gibbs energy change for the formation of 2 mol of $(A-B)$ pairs is expended in terms of the pair fractions:

$$\Delta g_{AB} = \Delta g_{AB}^{\circ} + \sum_{i\geq 1} g_{AB}^{i0}(X_{AA})^i + \sum_{j\geq 1} g_{AB}^{0j}(X_{BB})^j \tag{9}$$

Δg_{AB}°, g_{AB}^{i0} and g_{AB}^{0j} are the temperature dependant model parameters that are optimized in this work for the As–Co and As–Fe systems. The coordination numbers can be varied with composition to reproduce the SRO, as given by equations (10) and (11). The composition of maximum SRO is determined by the ratio Z_B/Z_A:

$$\frac{1}{Z_A} = \frac{1}{Z_{AA}^A}\left(\frac{2n_{AA}}{2n_{AA}+n_{AB}}\right) + \frac{1}{Z_{AB}^A}\left(\frac{2n_{AB}}{2n_{AA}+n_{AB}}\right) \tag{10}$$

$$\frac{1}{Z_B} = \frac{1}{Z_{BB}^B}\left(\frac{2n_{BB}}{2n_{BB}+n_{AB}}\right) + \frac{1}{Z_{BA}^B}\left(\frac{2n_{AB}}{2n_{BB}+n_{AB}}\right) \tag{11}$$

Z_{AA}^A and Z_{AB}^A are the coordination numbers when the nearest neighbours of an A atom are A atoms and B atoms respectively. Z_{BB}^B and Z_{BA}^B are defined similarly. In this work, Z_{AsAs}^{As}, Z_{CoCo}^{Co} and Z_{FeFe}^{Fe} are set to be 6 for consistency with previous work. Analyzing the measured activity data in both As–Co and As–Fe binary systems (Fig. 4 b) and Fig. 5b)) shows that the maximum SRO occurs at approximately a composition of 45 at. % As. The coordination numbers Z_{AsCo}^{As} and Z_{AsFe}^{As} are set to be 6, and Z_{AsCo}^{Co} and Z_{AsFe}^{Fe} are set to be 5 in this work.

3.2. Thermodynamic model for the liquid phase in the As–Fe–S ternary system

Geometric models can be used to estimate the excess Gibbs energy of a ternary system from the parameters of the three binary subsystems [130,131]. For a given geometric model, the excess Gibbs energy of the ternary system at any composition p is calculated from the binary parameters at points a, b and c. The difference between the models is the placement of these three points. Since the binary excess Gibbs energy in As–Fe and As–S systems depend strongly upon composition, the different models will give very different results. Thus, the choice of points a, b and c is very important to correctly interpolate the ternary As–Fe–S system. Since Fe is a transition metal and exhibits different properties from As and S, the use an asymmetric model is more reasonable. In this work, the Toop type of interpolation technique was used to optimize the ternary As–Fe–S liquid phase, with iron as the asymmetric component.

3.3. Thermodynamic model for solid solutions

The Compound Energy Formalism (CEF) [13] is used to model the solid solutions. For As–Co and As–Fe binary systems, a magnetic contribution to the Gibbs energy was added to describe the cobalt and iron rich solid solutions. For the ternary solid solutions, the sublattice models considered in this work are presented in Table 4 and justified in this section. The solubility of As in $Fe_{1-x}S$ as well as the solubility of S in Fe_2As and FeAs are neglected in the present work.

3.3.1. Co and Fe rich solid solutions

Since cobalt and iron exhibits magnetic ordering, an additional term can be added to the Gibbs energy to include the magnetic contribution. Inden [132] derived the following equation:

$$G^{magnetic} = RT\ln(\beta+1)f(\tau) \tag{12}$$

β corresponds to the average magnetic moment per mole of atoms in Bohr magnetons and τ corresponds to the ratio of the temperature and the critical temperature of magnetic ordering. For ferromagnetic elements, the critical temperature corresponds to the Curie temperature T_C. For antiferromagnetic elements, the critical temperature corresponds to the Néel temperature T_N. The expression $f(\tau)$ was subsequently simplified by Hillert and Jarl [133] by expanding it into a power series. For the ferromagnetic Co and Fe, T_C and β can be expressed as a function of composition. For each disordered phase in the Fe–As system, T_C and β are given by the following expressions:

$$T_{C(x)} = x_{Fe}T_C(Fe) + T_C^{Excess} \text{ with } T_C^{Excess} = x_{Fe}x_{As}\sum_{i=0\ldots n} T_C(x_{As}-x_{Fe})^i \tag{13}$$

$$\beta(x) = x_{Fe}\beta(Fe) + \beta^{Excess} \text{ with } \beta^{Excess} = x_{Fe}x_{As}\sum_{i=0\ldots n} \beta(x_{As}-x_{Fe})^i \tag{14}$$

The expansion parameters T_C and β are evaluated based on the experimental data available. The same expressions can be derived for cobalt [134].

3.3.2. FeS_2

Electron microscopy and X-ray absorption spectroscopy studies on natural FeS_2 samples indicate a preferential substitution of arsenic into sulfur atomic positions [102,106,135–141]. This substitution mechanism usually occurs at reduced conditions such as in orogenic gold deposits [101,142,143]. XANES measurements on gold-bearing pyrite by Simon et al. [138] showed that arsenic is present in FeS_2 as As^{-1} and it substitutes for sulfur in the S_2^{-2} units as AsS^{-2} pairs. Blanchard et al. [144] investigated the arsenic substitution mechanism in FeS_2 using DFT. Their results also suggest that the formation of AsS dianion groups

Table 5
Heat capacities of the solid phases in this work.

Phases	T range, K	$C_p(T)$, J/(mol.K)
Co_5As_2	298.15–1196.15	$172.0593 + 0.03741191T - 771670T^{-2} + 5.2044 \times 10^{-6}T^2$
Co_2As (LT)	298.15–725.15	$73.4866 + 0.016051216T - 313308T^{-2} + 2.08176 \times 10^{-6}T^2$
Co_2As (HT)	725.15–1090	$73.4866 + 0.016051216T - 313308T^{-2} + 2.08176 \times 10^{-6}T^2$
	1090–1230.15	$79.388237 + 0.01618956T - 290108T^{-2} + 2.08176 \times 10^{-6}T^2$
Co_3As_2	298.15–1090	$121.8871 + 0.026792954T - 481562T^{-2} + 3.12264 \times 10^{-6}T^2$
	1090–1230.15	$133.690374 + 0.015928434T - 435162T^{-2} + 3.12264 \times 10^{-6}T^2$
CoAs (LT)	298.15–1090	$48.4005 + 0.010741738T - 168254T^{-2} + 1.04088 \times 10^{-6}T^2$
	1090–1248.15	$54.3021 + 0.005309478T - 145054T^{-2} + 1.04088 \times 10^{-6}T^2$
CoAs (HT)	1248.15–1453.15	$54.3021 + 0.005309478T - 145054T^{-2} + 1.04088 \times 10^{-6}T^2$
$CoAs_2$ (LT)	298.15–800	$71.7149 + 0.016173998T - 191454T^{-2} + 1.04088 \times 10^{-6}T^2$
$CoAs_2$ (HT)	800–1090	$71.7149 + 0.016173998T - 191454T^{-2} + 1.04088 \times 10^{-6}T^2$
	1900–1193.15	$83.518174 + 0.005309478T - 145054T^{-2} + 1.04088 \times 10^{-6}T^2$
$CoAs_3$	298.15–1100	$82.39189 + 0.038517T + 8.48 \times 10^{-7}T^2$
$FeAs_2$	298.15–1300	$76.69 + 0.0031T - 603000T^{-2}$
FeAs	298.15–1300	$102.9396 - 0.0385038T + 287228.09T^{-2} + 3.2524 \times 10^{-5}T^2 - 821.217T^{-0.5}$
Fe_3As_2	298.15–1090	$120.6217 + 0.03340964T - 510554T^{-2} + 1.060686 \times 10^{-6}T^2$
	1090–1811	$132.4249 + 0.02254512T - 464154T^{-2} + 1.060686 \times 10^{-6}T^2$
Fe_2As	298.15–1090	$72.643 + 0.02046234T - 332636T^{-2} + 7.07124 \times 10^{-7}T^2$
	1090–1212	$78.5446 + 0.01503008T - 309436T^{-2} + 7.07124 \times 10^{-7}T^2$
FeAsS	1090–1000	$75.51 + 0.00478T - 754300T^{-2}$

is energetically the most favorable. Substitution of arsenic into iron atomic positions was also reported. This substitution mechanism is less common and observed mainly at oxidised conditions in hydrothermal deposits [101,142,143]. In a hydrothermal gold deposit, Deditius et al. [142] observed arsenic substituting iron as As^{3+}. Qian et al. [145] synthetized FeS_2 for temperatures of 398 K and 493 at the saturation pressure and their analyses suggest that arsenic substitutes for iron in FeS_2. In this work, the FeS_2 solid solution is modeled considering the preferential substitution of arsenic into sulfur atomic positions as presented in Table 4.

3.3.3. *FeAsS*

Möller and Kersten [146] showed that the conductivity of AsFeS depends on the As/S ratio. The substitution of sulfur by arsenic has been shown using X-ray spectroscopies by Savage et al. [139] and Le Pape et al. [140,147]. This substitution results in a p-type conductivity [146]. In arsenopyrite enriched in sulfur, sulfur substitute for arsenic according to the electron microprobe results obtained by Nesbitt et al. [148]. This substitution results in an n-type conductivity [146]. Like in $FeAs_2$, Tossell et al. [149] and Nesbitt et al. [148] suggest that sulfur and arsenic form pairs of atoms occurring as AsS^{2-} in AsFeS. The measurements of Clark [61] and Kretschmar and Scott [95] on natural samples shown in Fig. 6 d) indicate a deviation towards the arsenic rich side but below 673 K, Kretschmar and Scott [95] explain that uncertainty still remains in the sulfur rich side of AsFeS. In this work, the AsFeS solid solution is modeled by considering both substitution mechanisms and the sublattice model is presented in Table 4.

3.3.4. *$FeAs_2$*

The structure of $FeAs_2$ derives from the structure of FeS_2 (marcasite), where arsenic is substituted for sulfur [96,150] as modeled in this work.

4. Results and discussions

The optimization was conducted using the FactSage™ thermochemical software. The As–Co, As–Fe and As–Fe–S systems are assessed based on the literature data presented in the previous sections, and the optimized thermodynamic model parameters are presented in Table 6. The enthalpies of formation of the compounds of the As–Co system from thermodynamic tables and DFT calculations are shown in Fig. 1 a), along with the optimized values from this work. For compounds of the As–Fe system, the enthalpies of formation from measurements and DFT calculations are shown in Fig. 1 b), along with the optimized values from this work. To best reproduce the phase diagram and the activity data, the selected enthalpy of formation values for Fe_2As and FeAs are slightly higher than the values measured by Stolyarova [82,83]. The values suggested by Espelata et al. [30] and the ones estimated by the Miedema model [42,43,84] are not considered reliable in the context of this work and therefore not included in the Figures. The thermodynamic properties proposed in this work for Fe_3As_2 have a significant uncertainty due to the lack of data et the doubt surrounding its existence.

The heat capacity (C_p) curves of the intermediate compounds of both binary systems are presented in Fig. 2 and the functions are presented in Table 5. The Neumann-Kopp rule was used to estimate the heat capacity of the compounds with no measured data. For $FeAs_2$, the calculated heat capacity curve corresponds to the estimation of Perfetti et al. [81] by analogy with the heat capacity of isostructural FeS_2 (marcasite) and FeAsS (arsenopyrite). Since the heat capacity of FeAs derived by Gonzalez-Alvarez et al. [69] from enthalpy increment have a higher uncertainty, the calculated curve is based on the measurements obtained using adiabatic calorimetry. The standard entropies ($S^o_{298.15\ K}$) of the As–Co compounds from thermodynamic tables and the selected values in this work are presented in Fig. 3 a). The standard entropies ($S^o_{298.15\ K}$) of the As–Fe compounds based on C_p measurements and the selected values in this work are presented in Fig. 3 b). Due to the uncertainties surrounding the thermal dissociation experiments performed by Kochnev [48], their results were not used to optimize the properties of the As–Co compounds. The thermodynamic properties of the phases were optimized to reproduce the phase diagram data and the activity measurements shown in Fig. 4.

The calculated binary phase diagrams are shown in Fig. 4 a) and Fig. 5a). For compounds undergoing polymorphic transformations, the enthalpies of transformations reported in the literature are used in this work and the different phases are identified as LT (low temperature) or HT (high temperature). The calculated phase diagrams are in good agreement with the experimental data. To optimize the cobalt rich side of the As–Co system, the measurements from Friedrich [22] and Koster [24] are selected since their measured eutectic temperature and composition are in good agreement, contrary to the data by Hashimoto [23] suggesting a much higher eutectic temperature. To optimize the magnetic parameter for the As–Co system, the data from Koster [24] ia selected. The calculated magnetic transformations in both As–Co and As–Fe systems are shown in the same Figures. Since there is a lack in information on the excess magnetic moment, the excess contribution to

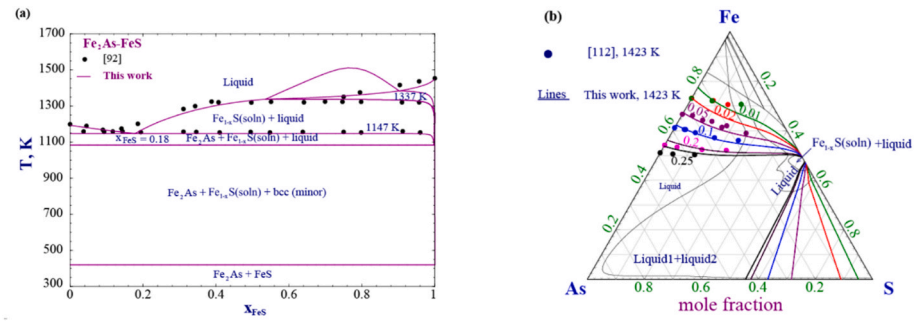

Fig. 7. Calculated **a)** pseudo-binary *Fe_2As-FeS* system **b)** isothermal section of the As–Fe–S system at 1423 K along with the calculated and the experimental liquid As iso-activity curves.

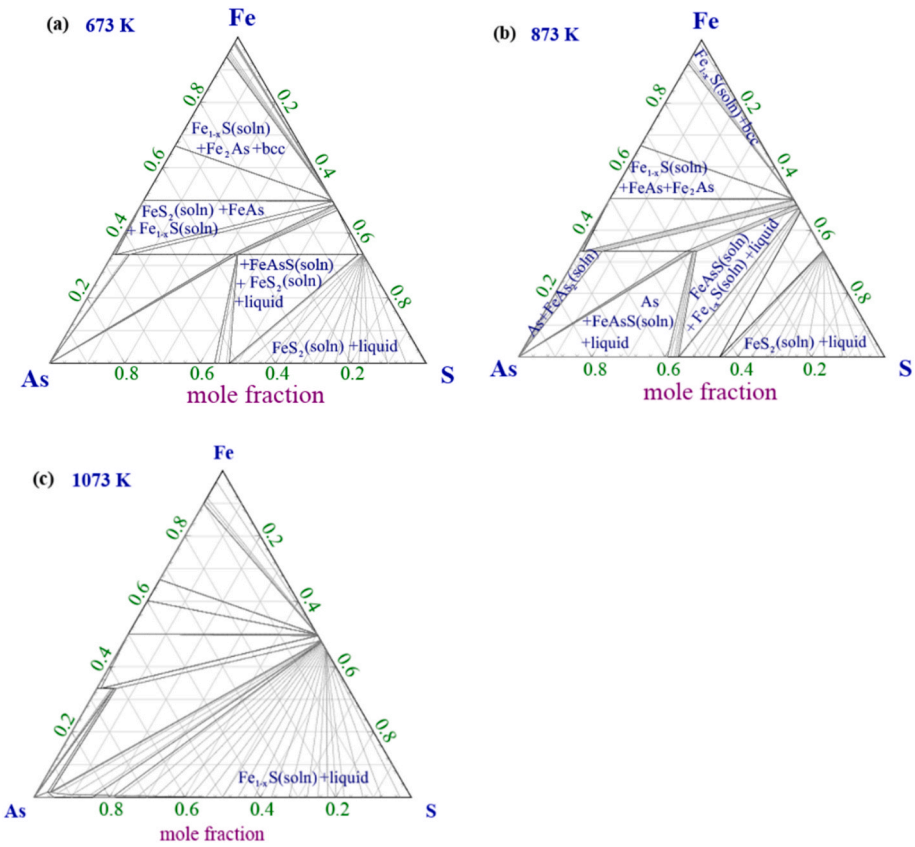

Fig. 8. Calculated **a)** isothermal section at 673 K, **b)** 873 K, **c)** 1073 K.

the β term is considered nonsignificant in this work for both systems and only the T_C^{Excess} parameters are optimized. This simplified model gives adequate results as seen from the Figures. In this work, Co_5As_2 is stable only from 1141 K to 1192 K, in a range of about 50° like proposed by Ellner et al. [29]. Since the decomposition temperatures of $CoAs_2$ and $CoAs_3$ have not been measured, the proposed values in this work are uncertain. The calculated activities are presented in Fig. 4 b) and Fig. 5 b). To determine the activity of As, the thermodynamic properties used by Hino and Azakami [72] in their calculation are from Hultgren et al. [73]. The data is considered reliable in the context of this work, contrary to what was suggested by Botor [74]. For the As–Fe system, the calculated liquid enthalpy of mixing at 1123 K at the composition of 0.24 at. % As is −19.1 kJ/mol, slightly higher than the measured values of Wypartowicz et al. [79].

For the ternary FeAsS compound, the calculated heat capacity curve is based on the measurements of Pashinkin et al. [113] as seen from Fig. 6 a). The standard entropy of 68.5 J/(mol.K) by the same authors is selected in this work. The standard enthalpy of formation is −139.9 kJ/mol to reproduce the decomposition temperature of the compound at 975 ± 3 K as measured by Clark [61]. Fig. 6 b) and 6 c) show that the optimized thermodynamic properties of FeAsS reproduce well the vapor pressure data and the equilibrium of reaction 1. The calculations shown in Fig. 6 b) and 6 c) are performed for a stoichiometric FeAsS composition even if some of the reported data are from FeAsS samples with compositions that deviate from stoichiometry. Even if FeAsS exists in nature in a variable composition range, only the measurements of Clark [61] and Kretschmar and Scott [95] are considered in this work to model the limits of the solid solution. Fig. 6 d) presents the homogeneity range of FeAsS along the FeS_2-$FeAs_2$ join. Some phases are present at equilibrium in minor quantities in this join and are identified in the Figure with "(minor)". FeAsS decomposes at a temperature of 974 K and a composition of 38 at. % As, which agrees with the experimental measurements. It decomposes to form $Fe_{1-x}S$ solid solution, $FeAs_2$ solid solution and a minor quantity of arsenic, and at a slightly higher

Table 6
Optimized thermodynamic parameters for As–Co and As–Fe–S systems ($J\ mol^{-1}$).

Phases (model)	Thermodynamic parameters	References
Liquid **(MQM)** $(\mathbf{As},\mathbf{Co})(\mathbf{Va})$	$Z^{As}_{AsCo} = 6$; $Z^{Co}_{AsCo} = 5$; $Z^{As}_{AsAs} = Z^{Co}_{CoCo} = 6$ $\Delta g_{As-Co} = -25000 + 3.655T + 4000\ X_{AsAs} + (-15000 + 11.60787129)\ X^3_{CoCo}$	This work
Liquid **(MQM)** $(\mathbf{As},\mathbf{Fe},\mathbf{S})(\mathbf{Va})$	$Z^{As}_{AsFe} = 6$; $Z^{Fe}_{AsFe} = 5$; $Z^{As}_{AsS} = 3$; $Z^{S}_{AsS} = 2$; $Z^{As}_{AsAs} = Z^{Fe}_{FeFe} = Z^{S}_{SS} = 6$ $\Delta g_{As-S} = (-48\,000 + 88.067T - 9.155TlnT) + (-30\,000 + 92.124T - 10.072TlnT)$ $X_{AsAs} + (-74000 + 249.331T - 27.092TlnT)X^2_{AsAs} + (52\,500–23.053)X^3_{AsAs} + 3\,000X_{SS}$ $+2500\ X^3_{SS}$ $\Delta g_{As-Fe} = -25090 + 6.1T - 5TX_{AsAs} - 5500\ X_{FeFe} - 1.936\ X^3_{CoCo}$ $\Delta g_{Fe-S} = -104.888 + 0.338T + (35.043 - 9.880T)X_{FeFe} + 23.972T\ X^2_{FeFe} + 30.437$ $X^3_{FeFe} + (8.626T)X_{FeFe} + (72.954–26.178T)\ X^2_{SS} + 25.106\ X^4_{SS}$ $g^{101}_{FeS(As)} = -25000$ $g^{102}_{FeS(As)} = 40000$ $g^{103}_{FeS(As)} = -11000$ $g^{001}_{AsFe(S)} = 13200$	[21] This work [20] This work
Fcc(A1) (CEF) $(\mathbf{As},\mathbf{Co},\mathbf{Fe},\mathbf{S})_1(\mathbf{Va})_1$	${}^0L_{As,Co:Va} = -61000 + 10.072T$ $T^E_C = -1354.057X_{As}X_{Co}$ ${}^0L_{Fe,As:Va} = -75000 + 22.912T$ ${}^0L_{Fe,S:Va} = -59070.737 - 34.612T$	This work This work [20]
Bcc(A2) (B–W) $(\mathbf{As},\mathbf{Fe},\mathbf{S})_1(\mathbf{Va})_3$	${}^0L_{Fe,As:Va} = -77000 + 22.986T$ $T^E_C = 549.252X_{As}X_{Fe} - 150X_{As}X_{Fe}(X_{As} - X_{Fe})^1$ ${}^0L_{Fe,S:Va} = -31.041 - 10.657T$	This work [20]
Hcp (A3) (CEF) $(\mathbf{As},\mathbf{Co})_1(\mathbf{Va})_{0.5}$	${}^0L_{As,Co:Va} = -58905$	This work
hP4-$Fe_{1-x}S$ (CEF) $(\mathbf{Fe},\mathbf{Va})_1(\mathbf{S})_2$	${}^0G_{Fe:S} = -96291.00 - 21.991T + GHSER_{Fe} + 2GHSER_S$ [a] ${}^0G_{Va:S} = 140049.39 + 32.086 + 2GHSER_S$ [a] ${}^0L_{Fe,Va:S} = -225830.67 - 26.359T$	[20]
Fe_3As_2 (CEF) $(\mathbf{Fe})_3(\mathbf{As},\mathbf{Va})_2$	${}^0G_{Fe:As} = -75300 + 28.867T + 3GHSER_{Fe} + 2GHSER_{As}$ ${}^0G_{Fe:Va} = 72448.5 - 44.975T + 3GHSER_{Fe}$ ${}^0L_{(Fe:As,Va)} = 56000 - 52.190T$	This work
cP12-FeS_2(CEF) $(\mathbf{Fe})_1(\mathbf{S},\mathbf{As})_2$	${}^0G_{Fe:S} = -171048.025 - 38.490T + GHSER_{Fe} + 2GHSER_S$ [a] ${}^0G_{Fe:As} = -75772 + 17.659T + GHSER_{Fe} + 2GHSER_{As}$ ${}^0L_{(Fe:S,As)} = -25000$	[20] This work
oP6-$FeAs_2$(CEF) $(\mathbf{Fe},\mathbf{Va})_1(\mathbf{As},\mathbf{S})_2$	${}^0G_{Fe:As} = -85772 + 17.659T + GHSER_{Fe} + 2GHSER_{As}$ ${}^0G_{Fe:S} = -154500 + 37.51T + GHSER_{Fe} + 2GHSER_S$ ${}^0G_{Va:As} = 20000 + 2GHSER_{As}$ ${}^0G_{Va:S} = 860082.627 - 19.251T + 2GHSER_S$ ${}^0L_{(Fe:As,S)} = -48500$	This work
mP12-FeAsS (CEF) $(\mathbf{Fe})_1(\mathbf{As},\mathbf{S})_1(\mathbf{S},\mathbf{As})_1$	${}^0G_{Fe:As:S} = -139\,900 + 27.510T + GHSER_{Fe} + GHSER_{As} + GHSER_S$ ${}^0G_{Fe:As:As} = -51272 - 17.280 + GHSER_{Fe} + 2GHSER_{As}$ ${}^0G_{Fe:S:S} = -81048 + 38.490T + GHSER_{Fe} + 2GHSER_S$ ${}^0G_{Fe:S:As} = -89900 + 26.539 + GHSER_{Fe} + GHSER_{As} + GHSER_S$ ${}^0L_{(Fe:As:S:As)} = 6000 - 38.805T$	This work

[a] Heat capacity functions given in Table 5 of reference [20].

Table 7
Summary of some invariant reactions involving the liquid phase in the ternary *As-Fe-S* system.

Reactions			Temperatures
at. % **Fe**	at. % **S**	at. % **As**	**K** (°C)
Liquid ⇌Liquid 2 + $Fe_{1-x}S$+ bcc			
0.629	0.318	0.053	1233.3 (960.15)
0.629	0.085	0.170	
Liquid 1 ⇌ $Fe_{1-x}S$ + bcc + Fe_2As			
0.465	0.131	0.404	1220 (946.85)
Liquid ⇌ Fe_2As+ $Fe_{1-x}S$ + bcc			
0.735	0.032	0.233	1083.14 (809.99)

temperature, the equilibrium becomes $Fe_{1-x}S$ solid solution, $FeAs_2$ solid solution and liquid. This is in accordance with the measurements performed in the presence of vapor by Clark [61] and Barton [80]. The calculations also show that the AsFeS solid solution is in equilibrium with $FeAs_2$ solid solution and arsenic in the arsenic rich side. In the sulfur rich side, the AsFeS solid solution is in equilibrium with $Fe_{1-x}S$ solid solution and liquid above 772 K. Below this temperature, the equilibrium exists with FeS_2 solid solution and liquid. This corresponds to the equilibrium suggested by Clark [61] at 764 ± 12 K. The FeAsS + FeS_2 + As equilibrium line suggested at 636 ± 50 K by Barton [80] is not obtained in the present work. The maximum solubility of S in $FeAs_2$ measured by Clark [61] is reproduced as seen from Fig. 6 d). The maximum solubility of As in FeS_2 is set to 2 at. % As.

The liquid phase is modeled with four ternary parameters, presented in Table 6, to reproduce accurately the experimental data. The pseudo-binary Fe_2As-FeS is presented in Fig. 7 a). The calculated eutectique temperature is 1147 K and the eutectique composition is 18 mol % FeS, slightly lower than the composition of 22.5 mol % FeS suggested by Nishihara and Izaki [92]. The calculated monotectic reaction occurs at a temperature of 1337 K. The isotherm at 1423 K is also shown in Fig. 7 b) along with the As iso-activity curves with liquid arsenic as the standard

state. The calculated curves are in good agreement with the measurements of Hino [112]. The calculated isothermal sections at 673 K, 873 K and 1073 K presented in Fig. 8 are in excellent agreement with the work of Clark [61] and Barton [80]. A summary of the invariant reactions involving four-phase intersection points with liquid in the ternary As-Fe-S system is presented in Table 7.

5. Conclusion

In this work, the thermodynamic information available in the literature is critically evaluated and used to optimize the As–Co and the As–Fe binary systems. Important uncertainties remain due to the lack of experimental data in the arsenic rich regions of both phase diagrams. The binary systems are assessed based on all available literature data to propose a reasonable set of model parameters for the arsenic rich region. The MQM with the pair approximation is applied to model the liquid phase. This model is well adapted to introduce extra parameters in X (As–As) pairs that can be adjusted with minimal impact on the rest of the optimization, contrary to the correlated Redlich-Kister parameters. For the ternary As–Fe–S, the Toop interpolation technique was used with iron as the asymmetric component. The CEF was used for solid solutions, with added magnetic contributions to describe the Gibbs energy of cobalt and iron rich solid solutions. The calculated phase diagrams and thermodynamic properties provide an accurate description of all reliable experimental data.

Declaration of competing interest

The authors declare the following financial interests/personal relationships which may be considered as potential competing interests: Patrice Chartrand is co-developper of the FactSage thermochemical software package.

Data availability

Data will be made available on request.

Acknowledgments

The authors would like to thank the financial support from NSERC and CRC programs.

Appendix A. Supplementary data

Supplementary data to this article can be found online at https://doi.org/10.1016/j.calphad.2023.102589.

References

[1] Q. Dehaine, L.T. Tijsseling, H.J. Glass, T. Törmänen, A.R. Butcher, Geometallurgy of cobalt ores: a review, Miner. Eng. 160 (2021), 106656.
[2] P.S. Hooda, Trace Elements in Soils, Wiley, Chichester, 2010.
[3] S.S. Afolabi, M.O. Zakariyah, M.H. Abedi, W. Shafik, A survey on cobalt metallurgical processes and its application, J. Indian Chem. Soc. 98 (2021), 100179.
[4] H. Abdollahi, R. Saneie, S.Z. Shafaei, M. Mirmohammadi, A. Mohammadzadeh, O.H. Tuovinen, Bioleaching of cobalt from magnetite-rich cobaltite-bearing ore, Hydrometallurgy 204 (2021), 105727.
[5] H.A.E. Sayed, A.M.E. Naggar, B.H. Heakal, N.E. Ahmed, S. Said, A.A. Abdel-Rahman, Deep catalytic desulphurization of heavy gas oil at mild operating conditions using self-functionalized nanoparticles as a novel catalyst, Fuel 209 (2017) 127–131.
[6] R.D. McKerracher, C.P.d. Leon, R.G.A. Wills, A.A. Shah, F.C. Walsh, A review of the iron–air secondary battery for energy storage, ChemPlusChem 80 (2015) 323–335.
[7] M.Z. Abzalov, T.S. Brewer, L.I. Polezhaeva, Chemistry and distribution of accessory Ni, Co, Fe arsenic minerals in the Pechenga Ni-Cu deposits, Kola Peninsula, Russia, Mineralogy and Petrology 61 (1997) 145.
[8] C.L. Corkhill, D.J. Vaughan, Arsenopyrite oxidation–A review, Appl. Geochem. 24 (2009) 2342–2361.
[9] E.C.D. Santos, M.P. Lourenço, L.G. Pettersson, H.A. Duarte, Stability, structure, and electronic properties of the pyrite/arsenopyrite solid–solid interface–A DFT study, J. Phys. Chem. C 121 (2017) 8042–8051.
[10] G.M. Mudd, Z. Weng, S.M. Jowitt, I.D. Turnbull, T.E. Graedel, Quantifying the recoverable resources of by-product metals: the case of cobalt, Ore Geol. Rev. 55 (2013) 87–98.
[11] A.D. Pelton, S.A. Degterov, G. Eriksson, C. Robelin, Y. Dessureault, The modified quasichemical model I—binary solutions, Metall. Mater. Trans. B 31 (2000) 651–659.
[12] A.D. Pelton, P. Chartrand, The modified quasi-chemical model: Part II. Multicomponent solutions, Metall. Mater. Trans. 32 (2001) 1355–1360.
[13] B. Sundman, J. Ågren, A regular solution model for phases with several components and sublattices, suitable for computer applications, J. Phys. Chem. Solid. 42 (1981) 297–301.
[14] C.W. Bale, P. Chartrand, S.A. Degterov, G. Eriksson, K. Hack, R.B. Mahfoud, J. Melançon, S. Petersen, FactSage thermochemical software and databases, Calphad 26 (2002) 189–228.
[15] C.W. Bale, E. Bélisle, P. Chartrand, S.A. Decterov, G. Eriksson, K. Hack, L.-H. Jung, Y.-B. Kang, J. Melançon, A.D. Pelton, C. Robelin, S. Petersen, FactSage thermochemical software and databases—recent developments, Calphad 33 (2009) 295–311.
[16] C.W. Bale, E. Bélisle, P. Chartrand, S.A. Decterov, G. Eriksson, A. Gheribi, K. Hack, I.-H. Jung, Y.-B. Kang, J. Melançon, A.D. Pelton, S. Petersen, C. Robelin, J. Sangster, P. Spencer, M.-A.V. Ende, Reprint of: FactSage thermochemical software and databases, 2010–2016, Calphad 55 (2016) 1–19.
[17] B. Pei, B. Björkman, B. Jansson, B. Sundman, Thermodynamic assessment of the Fe-as system using an ionic two-sublattice model for the liquid phase, Z. Metallkd 85 (1994) 171–177.
[18] M. Ohno, K. Yoh, Thermodynamic modeling of the system As–Fe combined with first-principles total energy calculations, J. Cryst. Growth 310 (2008) 2751–2759.
[19] Y. Xing, J. Brugger, A. Tomkins, Y. Shvarov, Arsenic evolution as a tool for understanding formation of pyritic gold ores, Geology 47 (2019) 335–338.
[20] P. Waldner, A.D. Pelton, Thermodynamic modeling of the Fe-S system, J. Phase Equilibria Diffus. 26 (2005) 23–38.
[21] O. Kidari, P. Chartrand, Thermodynamic evaluation and optimization of the Ag-as-S system, J. Phase Equilibria Diffus. (2023) 1–31.
[22] V.K. Friedrich, Equilibrium diagram of the cobalt-arsenic alloys, Metallurgie 5 (1908) 150–157.
[23] U. Haschimoto, Relation between the allotropic transformation of cobalt and some additional elements, J. Jpn. Inst. Metals 1 (1937) 177–190.
[24] W. Koster, W. Mulfinger, Die Systeme des Kobalts mit Bor, Arsen, Zirkon, Niob und Tantal, Z. Metallkunde 38 (1938) 348–350.
[25] M.J. Kochner, Solid solutions in the cobalt-arsenic system, Doklady Akad. Nauk S .S.S.R. 73 (1950) 1197–1199.
[26] M. Hino, T. Azakami, Arsenic activity in the molten Co-as system- thermodynamic study of molten arsenic aloys (4th report), Resources and materials 109 (1993) 785–790.
[27] M. Hansen, K. Anderko, Constitution of Binary Alloys, McGraw-Hill, New York, 1958.
[28] R.D. Heyding, L.D. Calvert, Arsenides of transition metals: the arsenides of iron and cobalt, Can. J. Chem. 55 (1957) 449–457.
[29] M. Ellner, E. Lukacevic, M. El-Borage, The structure and stability of Co5As2, J. Less Common. Met. 118 (1986) 327–333.
[30] A.K. Espeleta, K. Yamaguchi, K. Itagaki, Calorimetric study of some arsenides and antimonides (MxAsy and MxSby (M=Cu, Fe, Co, Ni)), Shigen-to-Soza 107 (1991) 658–663.
[31] R.P. Elliott, Constitution of Binary Alloys, First Supplement McGraw-Hill, 1965.
[32] A. Nylund, A. Roger, J.P. Senateur, R. Fruchart, Structural transitions between phosphides, arsenides and arsenophoshides of the composition M 2 P, M 2 As and M 2 (P 1—x as x), Monatshefte für Chemie/Chemical Monthly 102 (1971) 1631–1642.
[33] A. Kjekshus, K.E. Skaug, On the phases Cr2As, Fe2As, Co2As and Rh2As, Acta Chem. Scand. 26 (1972) 2554–2556.
[34] K. Selte, A. Kjekshus, On phase transitions between the MnP and NiAs type structures, Acta Chem. Scand. 27 (1973) 3195–3206.
[35] C. Griffin, A Text-Book of Inorganic Chemistry, 1917.
[36] J.C. Quesnel, R.D. Heyding, Transition metal arsenides: V. A note on the rhodium/arsenic system and the monoclinic diarsenides of the cobalt, Family Canadian Journal of Chemistry 40 (1962) 814–818.
[37] R. Darmon, M. Wintenberger, Structure cristalline de CoAs2, Bull. Mineral. 89 (1966) 213–215.
[38] A. Kjekshus, T. Rakke, High temperature studies of marcasite and arsenopyrite type compounds, Acta Chem. Stand. A 31 (1977) 517–529.
[39] T. Siegrist, F. Hulliger, High-temperature behavior of CoAs2 and CoSb2, J. Solid State Chem. 63 (1986) 23–30.
[40] N. Mandel, J. Donohue, The refinement of the crystal structure of skutterudite, CoAs3, Acta Crystallogr. Sect. B Struct. Crystallogr. Cryst. Chem. 27 (1971) 2288–2289.
[41] S.E. Vaisburd, T.F. Remen, Activities of components in arsenide melts of irin, cobalt and nickel, Russ. J. Phys. Chem. 42 (1968) 389–391.
[42] A.D. Niessen, F.R.D. Boer, R.D. Boom, P.F.D. Chatel, W.C.M. Mattens, A. R. Miedema, Model predictions for the enthalpy of formation of transition metal alloys II, Calphad 7 (1983) 51–70.
[43] M.W. Hisham, S.W. Benson, Correlations of heats of formation of the different valency states of solid, polyvalent binary metal compounds, J. Phys. Chem. 89 (1985) 3417–3425.

[44] G.B. Naumov, I.L.v. Khodakovskii, B.N. Ryzhenko, Handbook of Thermodynamic Data, U.S. Geological Survey, Water Resources Division, 1974.
[45] D.D. Wagman, W.H. Evans, V.B. Parker, R.H. Schumm, L. Halow, S.M. Bailey, L. Kenneth, R. Nuttal, Selected values for inorganic and C1 and C2 organic substances in SI units, J. Phys. Chem. Ref. Data 11 (1982) 37–38.
[46] A. Kubaschewski, C.B. Alcock, Tables of Metallurgical Thermochemistry, Elsevier Science & Technology Books, 1979.
[47] C.J. Smithells, E.A. Brandes, Smithells Metals Reference Book, seventh ed., 1992.
[48] M.I. Kochnev, Thermodynamic properties of cobalt arsenides Doklay Akademii nauk SSSR, Comptes rendus de l'Académie des sciences de l'URSS) 70 (1950) 433–435.
[49] J. Majzlan, S. Kiefer, K. Lilova, T. Subramani, A. Navrotsky, M. Tuhý, A. Vymazolova, D.A. Chareev, E. Dachs, A. Benisek, Calorimetric study of skutterudite (CoAs2. 92) and heazlewoodite (Ni3S2), Am. Mineral. 107 (2022) 22191–22225.
[50] The materials Project. https://materialsproject.org/. Accessed 26 December 2022.
[51] The Open Quantum Materials Database. https://oqmd.org/. Accessed 22 December 2022.
[52] W. Friedrich, W. Borchers, Eisen und Arsen, Metallurgie 4 (1907) 129–137.
[53] H. Sawamura, T. Sakari, T. Inoue, M. Uematsu, Fe-as system in the range of high arsenic, Tetsu-To-Hagane 39 (1953) 776–777.
[54] P. Oberhoffer, A. Gallaschik, Contribution to the knowledge of iron-arsenic alloys, Stahl Eisen 43 (1923) 398–400.
[55] W.D. Jones, The influence of diffusing elements upon the alpha-gamma inversion of iron, J. Iron Steel Inst. 130 (1934) 429–437.
[56] V.N. Svechnikov, V.N. Gridnev, Allotropic transformation in iron-arsenic and iron antimony alloys (in Russian), Metallurg 13 (1938) 13–19.
[57] H. Sawamura, T. Mori, An Investigation of Equilibrium Diagram of Fe-As-C System, Department of metallurgy Kyoto University Japan, 1952, pp. 129–144.
[58] H. Sawamura, T. Mori, A Supplement to Investigation of Equilibrium Diagram of Fe-As-C, Kyoto University Japan, 1954, pp. 182–189.
[59] V.N. Svchnikov, A.K. Shurin, A more precise determination of the equilibrium diagram of A Fe-as system, Ukrainian SSR 1 (1957) 27–29.
[60] V.N. Svechnikov, V.M. Pan, A.K. Shurin, The effect of phosphorous and arsenic on the parameter of the crystal lattice and hardness of iron (in Russian), Fiz. Met. Metalloved. 6 (1958) 662–664.
[61] L. Clark, The Fe-as-S system: phase relations and applications, Econ. Geol. 55 (1960) 1345–1381.
[62] B. Predel, M. Frebel, The precipitation behavior of α-mixed crystals of iron with arsenic and antimony (in German), Arch. für das Eisenhuttenwes. 42 (1971) 365–373.
[63] B. Bozic, Equilibrium phase diagram for the iron-arsenic system (in Serbian), Srpska Akademija Nauka i Umetnosti, Odeljenje Tehnickih Nauka 14 (1979) 1–16.
[64] V.F. Wever, Ueber den Einfluß der Elemente auf den Polymorphismus des Eisens, Arch. für das Eisenhuttenwes. 2 (1929) 739–748.
[65] B.I. Bozic, R.J. Lucic, Martensitic Transformation in iron-arsenic alloys, Journal od Materials Scieince 12 (1977) 751–756.
[66] G. Hagg, Rontgenographische Studien uber die binaren Systeme von Eisen mit Phosphor, Arsen, Antimon und Wismut Z. Krist. 68 (1928) 470–471.
[67] G. Hagg, X-ray studies on the system iron arsenid, Z. Kristallogr. 71 (1929) 134–136.
[68] A. Seitkan, G.I. Lampronti, R.N. Widmer, N.P.M. Casati, S.A.T. Redfern, Thermal behavior of iron arsenides under non-oxidizing conditions, ACS Omega 5 (2020) 6423–6428.
[69] D. Gonzalez-Alvarez, F. Grønvold, B. Falk, W.J.E. F, B. R, K. G, FeAs: heat capacity, enthalpy increments, other thermodynamic properties from 5 to 1350 K, and magnetic transition, J. Chem. Therm. 21 (1989) 363–373.
[70] M.J. Buerger, The crystal structure of lollingite: FeAs2, zeitschr, Kristallographie 82 (1932) 504–513.
[71] R.D. Heyding, L.D. Calvert, Arsenides of the transition metals III. A note on the higher arsenides of iron, cobalt and nickel can, J. Chem. (1960) 313–316.
[72] M. Hino, T. Azakami, Activities of molten iron-arsenic and nickel-arsenic binary alloys, Min. Met. Inst. Japan 96 (1980) 553–558.
[73] R. Hultgren, P.D. Desai, D.T. Hawkins, M. Gleiser, K.K. Kelley, D.D. Wagman, Selected Values of the Thermodynamic Properties of the Elements, American Society of Metals OH, 1973.
[74] J. Botor, A. Zajaczkowski, L. Dziewidek, G.H. Siderov, The arsenic activity in the liquid Z, Metall (Berlin) 82 (1991) 304–309.
[75] N.A. Gokcen, The as (Arsenic) system, Bulletin of Alloy Phase Diagrams 10 (1989) 11–22.
[76] Y. Dong, Y. Peng, S. Wei, Y. Zhu, Activity of arsenic in Fe-as melt, Iron Steel 21 (1986) 11–13.
[77] F. Tsukihashi, K. Kuroda, S. Arakawa, N. Sano, Activity coefficient of antimony and arsenic in molten iron and carbon saturated iron, Steel Res. 65 (1994) 53–57.
[78] W. Yan, Y. Yang, W. Chen, M. Barati, A. McLean, Thermodynamic assessment of arsenic in iron and nickel alloys, Ironmak. Steelmak. 44 (2016) 220–226.
[79] J. Wypartowicz, K. Fitzner, O.J. Kleppa, Standard enthalpy of formation of Cu3As and heats of mixing in the liquid systems Cu-As and Fe-As by direct combination high temperature drop calorimetry, J. Alloys Compd. 217 (1995) 1–4.
[80] P.B. Barton, Themochemical study of the system Fe-As-S, Geochem. Cosmochim. Acta 33 (1969) 841–857.
[81] E. Perfetti, G.S. Pokrovski, K. Ballerat-Busserolles, V. Majer, F. Gibert, Densities and heat capacities of aqueous arsenious and arsenic acid solutions to 350 °C and 300 bar, and revised thermodynamic properties of As(OH)3°(aq), AsO(OH)3°(aq) and iron sulfarsenide minerals, Geochimica et Cosmochimica 72 (2008) 713–731.
[82] T.A. Stolyarova, Enthalpies of formation of iron arsenides, Geokhimia 7 (1977) 1095–1098.
[83] T.A. Stolyarova, The enthalpy of formation of iron arsenide (Fe2As), Russian journal of physical chemistry, Translated from Zhurnal Fizichekoi Khimii 52 (1978) 898.
[84] J. Klingbeil, R. Schmid-Fetzer, Interaction of metals with AlAs and InAs: estimation of ternary Al-As-M and in-As-M phase diagrams, Calphad 13 (1989) 367–388.
[85] A.S. Pashinkin, V.A. Muratova, N.V. Moiseyev, J.V. Bazhenov, Heat capacity and thermodynamic functions of iron diarsenide in the temperature range 5 K to 300 K, J. Chem. Therm. 23 (1991) 827–830.
[86] B. Jansson, in: R.I.o. Technology (Ed.), Trita-Mac-234, Division of Physical Metallurgy, Stockholm, Sweden, 1984.
[87] P.E. Blochl, Projector augmented-wave method, Phys. Rev. B 50 (1994).
[88] J.P. Perdew, K. Burke, M. Ernzerhof, Generalized gradient approximation made simple, Phys. Rev. Lett. 77 (1996) 3865.
[89] T. Tanaka, N.A. Gokcen, Excess thermodynamic properties of dilute solutions, J. Phase Equil. 16 (1995) 10–15.
[90] V. Prostakova, D. Shishin, E. Jak, Thermodynamic optimization of the as–S system, Calphad 72 (2021).
[91] V. Raghavan, Phase Diagrams of Ternary Iron Alloys. Part 2. Ternary Systems Containing Iron and Sulphur, ASM International, New Delhi, 1987.
[92] K. Nishihara, T. Izaki, Fundamental studies on spices (1st report) equilibrium relations in the Fe2as-FeS system (in Japanese), Journal of the Mining and Metallurgical Society of Japan 78 (1962) 609–611.
[93] L. Clark, Year Book. The Fe-As-S System, Carnegie Institution of Washington, 1958.
[94] H. McKinstry, Mineral assemblages in sulfide ores; the system Cu-Fe-As-S, Econ. Geol. 58 (1963) 483–505.
[95] U. Kretschmar, S.D. Scott, Phase relations involving arsenopyrite in the system Fe-as-S and their application, Can. Mineral. 14 (1976) 364–386.
[96] S.R. Hem, E. Makovicky, F. Gervilla, Compositional trends in Fe, Co and Ni sulfarsenides and their crystal-chemical implications: results from the Arroyo De La Cueva deposits, Ronda peridotite, Southern Spain, Can. Mineral. 39 (2001) 831–853.
[97] M. Wintenberger, Étude électrique et magnétique de composés sulfurés et arséniés d'éléments de transition. III. Propriétés électriques et magnétiques et liaisons dans l'arsénopyrite, la cobaltite et la loellingite, Bull. Mineral. 85 (1962) 107–119.
[98] N. Morimoto, L.A. Clark, Arsenopyrite crystal-chemical relations. American Mineralogist, Journal of Earth and Planetary Materials 46 (1961) 1448–1469.
[99] D.D. Klemm, Synthesen und Analysen in den Dreiecksdiagrammen FeAsS-CoAsS-NiAsS und FeS2-CoS2-NiS2, Neues Jahrbuch Mineral. Abhand. 103 (1965) 205–255.
[100] G. Simon, S.E. Kesler, S. Chryssoulis, Geochemistry and textures of gold-bearing arsenian pyrite, Twin Creeks, Nevada; implications for deposition of gold in carlin-type deposits, Econ. Geol. 94 (1999) 405–421.
[101] A.S. Stepanov, R.R. Large, E.S. Kiseeva, L.V. Danyushevsky, K. Goemann, S. Meffre, I. Zhukova, I. Belousov, Phase relations of arsenian pyrite and arsenopyrite, Ore Geol. Rev. 136 (2021), 104285.
[102] M. Reich, S.E. Kesler, S. Utsunomiya, C.S. Palenik, S.L. Chryssoulis, R.C. Ewing, Solubility of gold in arsenian pyrite, Geochem. Cosmochim. Acta 69 (2005) 2781–2796.
[103] M.A.A. Schoonen, H.L. Barnes, Reactions forming pyrite and marcasite from solution: I. Nucleation of FeS2 below 100 °C, Geochem. Cosmochim. Acta 55 (1991) 1495–1504.
[104] M.A.A. Schoonen, H.L. Barnes, Reactions forming pyrite and marcasite from solution: II. Via FeS precursors below 100 °C, Geochem. Cosmochim. Acta 55 (1991) 1505–1514.
[105] M.A.A. Schoonen, H.L. Barnes, Mechanisms of pyrite and marcasite formation from solution: III. Hydrothermal processes, Geochem. Cosmochim. Acta 55 (1991) 3491–3504.
[106] M.E. Fleet, A.H. Mumin, Gold-bearing arsenian pyrite and marcasite and arsenopyrite from carlin trend gold deposits and laboratory synthesis, Am. Mineral. 82 (1997) 182–193.
[107] S.R. Hem, E. Makovicky, The system Fe–Co–Ni–As–SI phase relations in the (Fe, Co, Ni) As0.5 S1.5 section at 650 and 500 C, Can. Mineral. 42 (2004) 43–62.
[108] M. Reich, U. Becker, First-principles calculations of the thermodynamic mixing properties of arsenic incorporation into pyrite and marcasite, Chem. Geol. 225 (2006) 278–290.
[109] N.K. Foley, R.A. Ayuso, Mineral sources and transport pathways for arsenic release in a coastal watershed, USA, Geochem. Explor. Environ. Anal. 8 (2008) 59–75.
[110] V. Ettler, Z. Johan, Mineralogy of metallic phases in sulphide mattes from primary lead smelting, Compt. Rendus Geosci. 335 (2003) 1005–1012.
[111] T. Mikuš, M. Chovan, O. Ponomarenko, S. Bondarenko, O. Grinchenko, Hydrothermal nickel mineralization from the black shales in Čierna lehota, Mineral. J. 35 (2013) 27–32.
[112] M. Hino, Activities of molten Cu-as, Cu-S-as and Fe-S-as alloys, J. Min. Metall. Inst. Jpn. 101 (1985) 543–548.
[113] A.S. Pahinkin, V.A. Muratova, A.M. Antukov, N.V. Moiseyev, Heat capacity and thermodynamic functiobs of arsenopyrite (in Russian), Neorg. Mater. 23 (1989) 221–224.

[114] P. Toulmin, P. Barton, A thermodynamic study of pyrite and pyrrhotite, Geochem. Cosmochim. Acta 28 (1964) 641–671.
[115] B.A. Strathdee, L.M. Pidgeon, Thermal decomposition and Vpour pressure measurements on arsenopyrite and an arsenical ore, Can. Min. Metall. Bull. 64 (1961) 883–887.
[116] N. Chakraborti, D.C. Lynch, Thermodynamics of roasting arsenopyrite, Metall. Trans. A B 14 (1983) 239–251.
[117] S. Fushimi, A.H. Webster, The Growth of Arsenopyrite Single Crystals by the Closed-Tube Iodine Vapour Transport Technique, Department of Energy, Mines and Resources, Mines Branch, Ottawa, Canada, 1969.
[118] G.N. Zviadadze, V.G. Rtskhiladze, Thermodynamics of the dissociation of arsenopyrite (in Russian), Soobsch. Acad. Nauk Gruz. SSR 33 (1964) 175–181.
[119] A.S. Pashinkin, V.A. Fedorov, G.N. Zviadidze, A.S. Malkova, A.P. Izergin, A. A. Izergin, S.A. Generalova, O.I. Dzhaparidze, L.A. Gelovani, Dissociation pressure of arsenopyrite and ivestigation of the Fe-as-S system (in Russian), Zh. Prikl. Khimii 52 (1979) 1085–1091.
[120] K.I. Chudnenko, Thermodynamic Modeling in Geochemistry: Theory, Algorithms, Software, and Applications, 2010 (in Russian), Novosibirsk.
[121] N.V. Vilor, L.A. Kaz'min, L.A. Pavlova, Aresenopyrite-pyrite paragenesis in gold deposits (thermodynamic modeling), Russ. Geol. Geophys. 55 (2014) 824–841.
[122] Y.V. Shvarov, HCh: new potentialities for the thermodynamic simulation of geochemical systems offered by Windows, Geochem. Int. 46 (2008) 834–839.
[123] A.S. Stepanov, Arsenic evolution as a tool for understanding formation of pyritic gold ores, Geology 47 (2019) e491.
[124] A.T. Dinsdale, SGTE data for pure elements, Calphad 15 (1991) 317–425.
[125] D.R. Stull, H. Prophet, JANAF Thermochemical Tables, U.S. Department of Commerce, Washington, DC, 1985.
[126] S.A. Degterov, A.D. Pelton, J.D. L'Ecuyer, Thermodynamic optimization of the selenium-arsenic (Se-As) system, J. Phase Equil. 18 (1997) 357–368.
[127] I. Barin, Thermochemical Data of Pure Substances, third ed. ed., VCH Verlag GmbH, Weinheim, Germany, 1995.
[128] A.D. Mah, Thermodynamic Data for Arsenic Sulfide Reactions Albany Research Center, Bureau of Mines, Albany, Oreg., 1982.
[129] I. Barin, O. Knacke, O. Kubaschewski, Thermochemical Properties of Inorganic Substances, Springer-Verlag, Berlin, Germany, 1977.
[130] A.D. Pelton, A general "geometric" thermodynamic model for multicomponent solutions, Calphad 25 (2001) 319–328.
[131] A.D. Pelton, Phase Diagrams and Thermodynamic Modeling of Solutions, Academic Press, 2018.
[132] G. Inden, The role of magnetism in the calculation of phase diagrams, Physica B 103 (1981) 82–100.
[133] M. Hillert, M. Jarl, A model for alloying in ferromagnetic metals, Calphad 2 (1978) 227–238.
[134] I. Ansara, N. Dupin, H.L. Lukas, B. Sundman, Thermodynamic assessment of the Al-Ni system, J. Alloys Compd. 247 (1997) 20–30.
[135] M.E. Fleet, S.L. Chryssoulis, P.J. MacLean, R. Davidson, C.G. Weisener, Arsenian pyrite from gold deposits; Au and as distribution investigated by SIMS and EMP, and color staining and surface oxidation by XPS and LIMS, Can. Mineral. 31 (1993) 1–17.
[136] A.L. Foster, G.E. Brown, T.N. Tingle, G.A. Parks, Quantitative arsenic speciation in mine tailings using X-ray absorption spectroscopy, Am. Mineral. 83 (1998) 553–568.
[137] V.L. Tauson, Gold solubility in the common gold-bearing minerals; experimental evaluation and application to pyrite, Eur. J. Mineral 11 (1999) 937–947.
[138] G. Simon, H. Huang, J.E. Penner-Hahn, S.E. Kesler, L.S. Kao, Oxidation state of gold and arsenic in gold-bearing arsenian pyrite, Am. Mineral. 84 (1999) 1071–1079.
[139] K.S. Savage, T.N. Tingle, P.A. O'Day, G.A. Waychunas, D.K. Bird, Arsenic speciation in pyrite and secondary weathering phases, Mother Lode gold district, Tuolumne County, California, Appl. Geochem. 15 (2000) 1219–1244.
[140] P. Le-Pape, M. Blanchard, J. Brest, J.C. Boulliard, M. Ikogou, L. Stetten, G. Landrot, G. Morin, Arsenic incorporation in pyrite at ambient temperature at both tetrahedral S–I and octahedral FeII sites: evidence from EXAFS–DFT analysis, Environ. Sci. Technol. 51 (2017) 150–158.
[141] F. Voute, S.G. Hagemann, N.J. Evans, C. Villanes, Sulfur isotopes, trace element, and textural analyses of pyrite, arsenopyrite and base metal sulfides associated with gold mineralization in the Pataz-Parcoy district, Peru: implication for paragenesis, fluid source, and gold deposition mechanisms, Miner. Deposita 54 (2019) 1077–1100.
[142] A.P. Deditius, S. Utsunomiya, D. Renock, R.C. Ewing, C.V. Ramana, U. Becker, S. E. Kesler, A proposed new type of arsenian pyrite: composition, nanostructure and geological significance, Geochem. Cosmochim. Acta 72 (2008) 2919–2933.
[143] C. Kusebauch, M. Oelze, S.A. Gleeson, Partitioning of arsenic between hydrothermal fluid and pyrite during experimental siderite replacement, Chem. Geol. 500 (2018) 136–147.
[144] M. Blanchard, M. Alfredsson, J. Brodholt, K. Wright, C.R.A. Catlow, Arsenic incorporation into FeS2 pyrite and its influence on dissolution: a DFT study, Geochem. Cosmochim. Acta 71 (2007) 624–630.
[145] G. Qian, J. Brugger, D. Testemale, W. Skinner, A. Pring, Formation of as (II)-pyrite during experimental replacement of magnetite under hydrothermal conditions, Geochem. Cosmochim. Acta 100 (2013) 1–10.
[146] P. Moller, G. Kersten, Electrochemical accumulation of visible gold on pyrite and arsenopyrite surfaces, Miner. Deposita 29 (1994) 404–413.
[147] P. Le-Pape, M. Blanchard, A. Juhin, J.-P. Rueff, M. Ducher, G. Morin, D. Cabaret, Local environment of arsenic in sulfide minerals: insights from high-resolution X-ray spectroscopies, and first-principles calculations at the as K-edge, J. Anal. At. Spectrom. 33 (2018) 2070–2082.
[148] H.W. Nesbitt, I.J. Muir, A.R. Prarr, Oxidation of arsenopyrite by air and air-saturated, distilled water, and implications for mechanism of oxidation, Geochem. Cosmochim. Acta 59 (1995) 1773–1786.
[149] J.A. Tossell, D.J. Vaughan, J.K. Burdett, Pyrite, marcasite, and arsenopyrite type minerals: crystal chemical and structural principles, Phys. Chem. Miner. 7 (1981) 177–184.
[150] J.M. Hartley, A.Z. Al-Bassam, R.C. Harris, G. Frisch, G.R. Jenkin, A.P. Abbott, Investigating the dissolution of iron sulfide and arsenide minerals in deep eutectic solvents, Hydrometallurgy 198 (2020), 105511.
[151] B. Hyde, M. Okeeffe, Marcasite and pyrite (FeS2), Aust. J. Chem. 49 (1996) 867–872.